Journal of Earth Science, *Vol. 35*, *No. 2*, *p. 430–448*, *April 2024*
Printed in China
https://doi.org/10.1007/s12583-021-1453-8
ISSN 1674-487X

Early Ordovician–Middle Silurian Subduction-Closure of the Proto-Tethys Ocean: Evidence from the Qiaerlong Pluton at the Northwestern Margin of the West Kunlun Orogenic Belt, NW China

Jinhong Xu[1, 2], Zhengwei Zhang*[1], Chengquan Wu*[1], Taiyi Luo[1], Weiguang Zhu[1], Xiyao Li[1], Ziru Jin[1], Pengcheng Hu[1]

1. *State Key Laboratory of Ore Deposit Geochemistry*, *Institute of Geochemistry*, *Chinese Academy of Sciences*, *Guiyang* 550018, *China*
2. *University of Chinese Academy of Sciences*, *Beijing* 100049, *China*

Jinhong Xu: https://orcid.org/0000-0002-6909-2738; Zhengwei Zhang: https://orcid.org/0000-0002-7989-0899; Chengquan Wu: https://orcid.org/0000-0002-8017-7185

ABSTRACT: Early Paleozoic magmatism in the West Kunlun Orogenic Belt (WKOB) preserves important information about the tectonic evolution of the Proto-Tethys Ocean. This paper reports whole-rock compositions, zircon and apatite U-Pb dating, and zircon Hf isotopes for the Qiaerlong Pluton (QEL) at the northwestern margin of WKOB, with the aim of elucidating the petrogenesis of the pluton and shedding insights into the subduction-collision process of this oceanic slab. The QEL is mainly composed of Ordovician quartz monzodiorite (479 ± 3 Ma), quartz monzonite (467–472 Ma), and syenogranite (463 ± 4 Ma), and is intruded by Middle Silurian peraluminous granite (429 ± 20 Ma) and diabase (421 ± 4 Ma). Zircon $\varepsilon_{Hf}(t)$ values reveal that quartz monzodiorites (+2.1 to +9.9) and quartz monzonites (+0.6 to +6.8) were derived from a mixed source of juvenile crust and older lower crust, and syenogranites (-5.6 to +4.5) and peraluminous granites (-2.9 to +2.0) were generated from a mixed source of lower crust and upper crust; diabases had zircon $\varepsilon_{Hf}(t)$ values ranging from -0.3 to +4.1, and contained 463 ± 5 Ma captured zircon and 1 048 ± 39 Ma inherited zircon, indicating they originated from enriched lithospheric mantle and were contaminated by crustal materials. The Ordovician granitoids are enriched in LILEs and light rare-earth elements, and depleted in HFSEs with negative Nb, Ta, P, and Ti anomalies, suggesting that they formed in a subduction environment. Middle Silurian peraluminous granites have the characteristics of leucogranites with high SiO_2 contents (74.92 wt.%–75.88 wt.%) and distinctly negative Eu anomalies (δEu = 0.03–0.14), indicating that they belong to highly fractionated granite and were formed in a post-collision extension setting. Comparative analysis of these results with other Early Paleozoic magmas reveals that the Proto-Tethys ocean closed before the Middle Silurian and its southward subduction resulted in the formation of QEL.

KEY WORDS: subduction-closure, Qiaerlong Pluton, West Kunlun Orogen, Proto-Tethys Ocean, tectonics, geochemistry.

0 INTRODUCTION

The West Kunlun orogenic belt (WKOB) is located between the Tarim Basin and the Qinghai-Tibet Plateau (Figure 1a; Zhang C L et al., 2019a; Pan, 2000). Two parallel and NW-SE trending large I-type magmatic suites (over 1 000 km) are distributed in the WKOB and provide important information on the tectonic evolution of the Early Paleozoic Proto-Tethys Ocean and Late Paleozoic Paleo-Tethys Ocean (Figure 1b, Zhang C L et al., 2019; Pan, 2000). Predecessors conducted a long-term and in-depth research on Early Paleozoic magmatism in this region, which has improved our understanding for tectonic evolution of the Proto-Tethys Ocean (Figure 1b; Zhang C L et al., 2019a; Xiao et al., 2002); however, some key issues remain controversial.

The Proto-Tethys Ocean was formed during the breakup of the Rodinia supercontinent and initially subducted from the Cambrian (Figure 1b; Zhang C L et al., 2019a; Xiao et al., 2002), but the closure time of the ocean are disputed as Early Silurian (Zhang C L et al., 2019b), Middle Silurian (Zhang Q C

*Corresponding authors: zhangzhengwei@mail.gyig.ac.cn; wuchengquan@mail.gyig.ac.cn

© China University of Geosciences (Wuhan) and Springer-Verlag GmbH Germany, Part of Springer Nature 2024

Manuscript received January 7, 2021.
Manuscript accepted March 15, 2021.

Xu Jinhong, Zhang Zhengwei, Wu Chengquan, Luo Taiyi, Zhu Weiguang, Li Xiyao, Jin Ziru, Hu Pengcheng, 2024. Early Ordovician–Middle Silurian Subduction-Closure of the Proto-Tethys Ocean: Evidence from the Qiaerlong Pluton at the Northwestern Margin of the West Kunlun Orogenic Belt, NW China. *Journal of Earth Science*, 35(2): 430–448. https://doi.org/10.1007/s12583-021-1453-8. http://en.earth-science.net

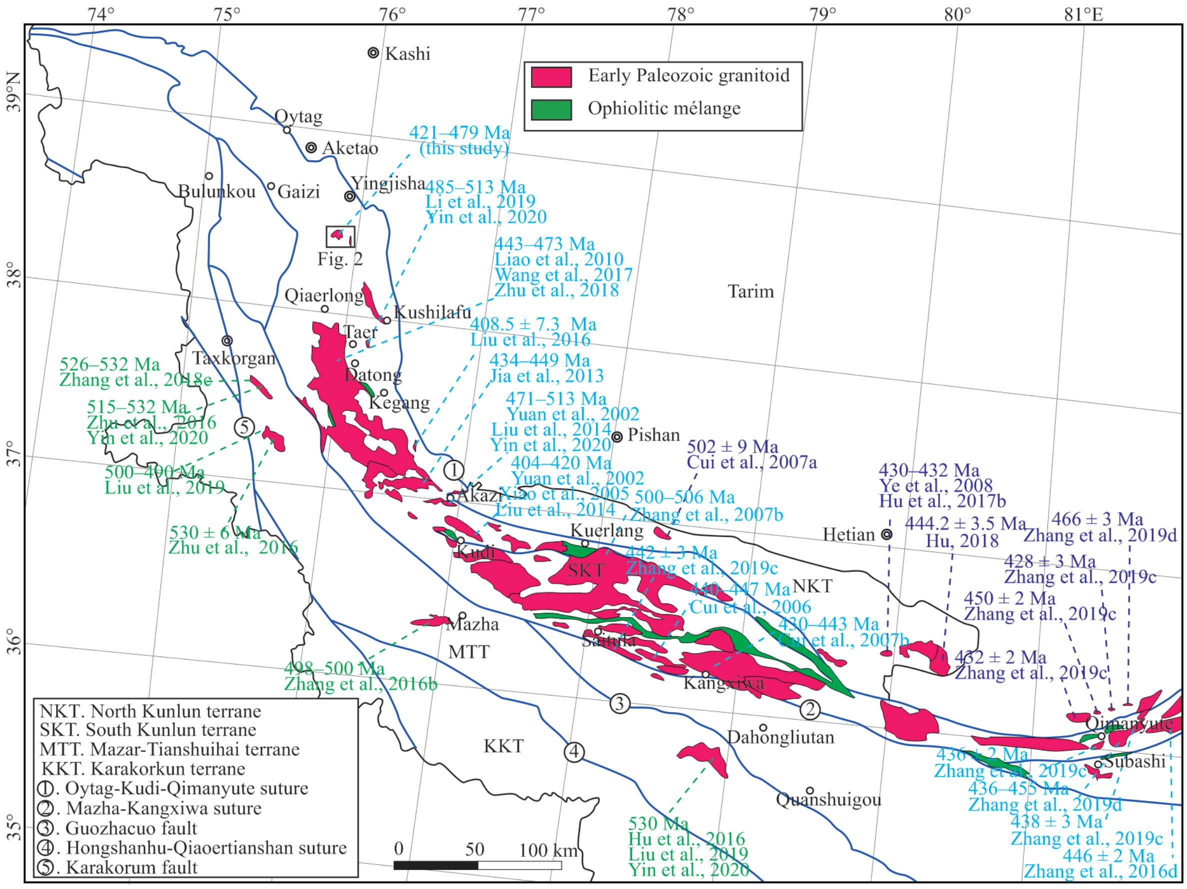

Figure 1. Simplified geological map of the West Kunlun orogenic belt (WKOB) (modified after Zhang et al., 2019a, b; Pan, 2000).

et al., 2019a; Ye et al., 2008), or Late Silurian (Li et al., 2019). Previous studies have shown that magmatism related to the Proto-Tethys Ocean was largely exposed in the southeastern part of the WKOB, while there are few reports of such magmatism in the northwestern margin of this area due to widely developed Jurassic–Cretaceous molasses (Robinson et al., 2004). The attribute of South Kunlun Terrane is widely debated, some have suggested that it was separated from the Tarim Block (Wang, 2004; Pan, 2000), while others have suggested that it is a huge subduction accretionary wedge (Zhang et al., 2018b; Xiao et al., 2005; Yuan et al., 2005). In addition, the subduction polarity of the Proto-Tethys ocean remained highly controversial whether it was southward (Li et al., 2019; Liu et al., 2019; Zhang Q C et al., 2019a, b, 2018; Jiang et al., 2002), northward (Wang, 2004; Xiao et al., 2000), or bidirectional (Wang et al., 2017; Xiao et al., 2002).

The Qiaerlong Pluton is exposed at the northwestern margin of the WKOB (Figure 1b). Previous studies reveal that this pluton is composed of fine-grained biotite granodiorite and medium-grained quartz diorite, and had apparent $^{206}Pb/^{238}U$ ages of 330 – 413 Ma (Henan Institute of Geological Survey, HIGS, 2005), indicating that the intrusion may be related to the Proto-Tethys Ocean. In this contribution, we present geological, whole-rock geochemical, zircon U-Pb, and Lu-Hf isotopic data for the Qiaerlong Pluton to decipher its crystallization ages and petrogenesis. These data are then combined with the results of previous research to better constrain the tectonic evolution of the Proto-Tethys Ocean.

1 GEOLOGICAL SETTING

Since the Phanerozoic, the WKOB experienced multiple opening, subduction, and closure processes of the Proto-Tethys, Paleo-Tethys, and Neo-Tethys Ocean, which led to multiple suture zones between different terranes, from north to south, including the Oytag-Kudi-Qimanyute Suture (OKQS) between the North Kunlun Terrane (NKT) and the South Kunlun Terrane (SKT); the Mazha-Kangxiwa-Subashi Suture Zone (MKSS) between SKT and the Mazar-Tianshuihai Terrane (MTT); and the Hongshanhu-Qiaoertianshan Suture (HQS) between MTT and the Karakorum Terrane (KKT) (Figure 1b; Zhang et al., 2019a; Wang et al., 2006; Pan, 2000).

The NKT is composed of a Paleoproterozoic basement and Neoproterozoic cover layers. The crystalline basement consists of the Paleoproterozoic Heluositan complex and the 2.41 Ga Akazi Pluton, and both underwent 1.9 Ga amphibolite- to granulite-facies metamorphism (Zhang C L et al., 2007). The cover layers comprise of the Neoproterozoic Sailajiazitage Group volcanic-sedimentary sequence and the Ailiankate Group clastic rocks which unconformably overlay the basement (Zhang C L et al., 2016).

The SKT is mainly composed of the Saitula Group and the Bulunkuole Group volcano-sedimentary sequences that all experienced 440 Ma amphibolite- to granulite-facies metamorphism (Zhang Q C et al., 2019a, b, 2018; Yuan et al., 2002). Some geologists believe that the Saitula Group and the Bulunkuole Group represent the Precambrian basement of SKT (Wang, 2004; Pan, 2000), while recent studies have shown they were deposited during the Early Paleozoic rather than the Late Neoproterozoic to Cambrian (Zhang et al., 2019a, b, 2018b), and have suggested that the SKT was a large accretionary wedge (Zhang et al., 2019a, b, 2018b; Yuan et al., 2002). This accretionary wedge included a seamount, arc volcano-sedimentary sequence, and Kudi ophiolite, formed via the southward subduction of the Proto-Tethys Ocean during the Early Paleozoic (Zhang et al., 2019a, b, 2018b; Yuan et al., 2002).

The MTT is a newly identified Precambrian terrane in the WKOB, and is mainly composed of crystallization basement rocks of the Mazar Complex (Zhang et al., 2018a, b) and is covered by the Tianshuihai Group (Zhang et al., 2018a, b). The Mazar Complex comprises 2.5 Ga bimodal volcanic rocks and sedimentary sequences, and underwent 2.0 Ga amphibolite-facies metamorphism (Zhang et al., 2018a, b; Ji et al., 2011). The Tianshuihai Group consists of a Late Paleozoic passive continental margin sedimentary sequence (Zhang et al., 2018b; Hu et al., 2016).

The KKT is mainly composed of Precambrian Heihezi Group basement rocks and a Paleozoic cover layer (Pan, 2000). The basement comprises crystalline schist, gneiss, quartzite, marble, phyllite, schist, and limestone, and the cover is a clastic-carbonate sedimentary sequence. However, the fundamental geological knowledge of the KKT is limited due to difficulties of access and harsh natural conditions.

Early Paleozoic magmatic rocks occur between the OKQS and the MKS in the WKOB, and are composed of abundant Cambrian–Ordovician I-type arc granites, Silurian high-Ba/Sr and A-type granites, and Kudi ophiolitic mélanges (Figure 1b; Xiao et al., 2002; Pan, 2000). The Kudi ophiolitic mélanges contain a Buziwan Valley ultramafic body, Yixieke volcanic rock, and flysch. Previous studies have revealed that the ultramafic body and volcanic rocks were crystallized during the Late Cambrian to Early Ordovician (Li and Zhang, 2014, and references therein) and were formed in an initial subduction setting (Yuan et al., 2005).

2 SAMPLING AND ANALYTICAL METHODS

2.1 Sampling

The Qiaerlong Pluton is located at the northwestern margin of the WKOB with an exposed area of 27 km^2 and is surrounded by the Late Carboniferous–Early Permian Tegeinaiqikedaban Formation to the west, the Early Carboniferous Talong Group to the east, the Late Carboniferous Kuerliang Group to the north and south (Figure 2a, HIGS, 2005). Field investigations reveal that the Qiaerlong Pluton is composed of quartz monzodiorite, quartz monzonite, and is invaded by syenogranite, peraluminous granite and diabase (Figures 2b, 3). However, detailed field relationship and outcropping range of different phases are still unclear due to the difficulties of access and harsh natural conditions of the studied area.

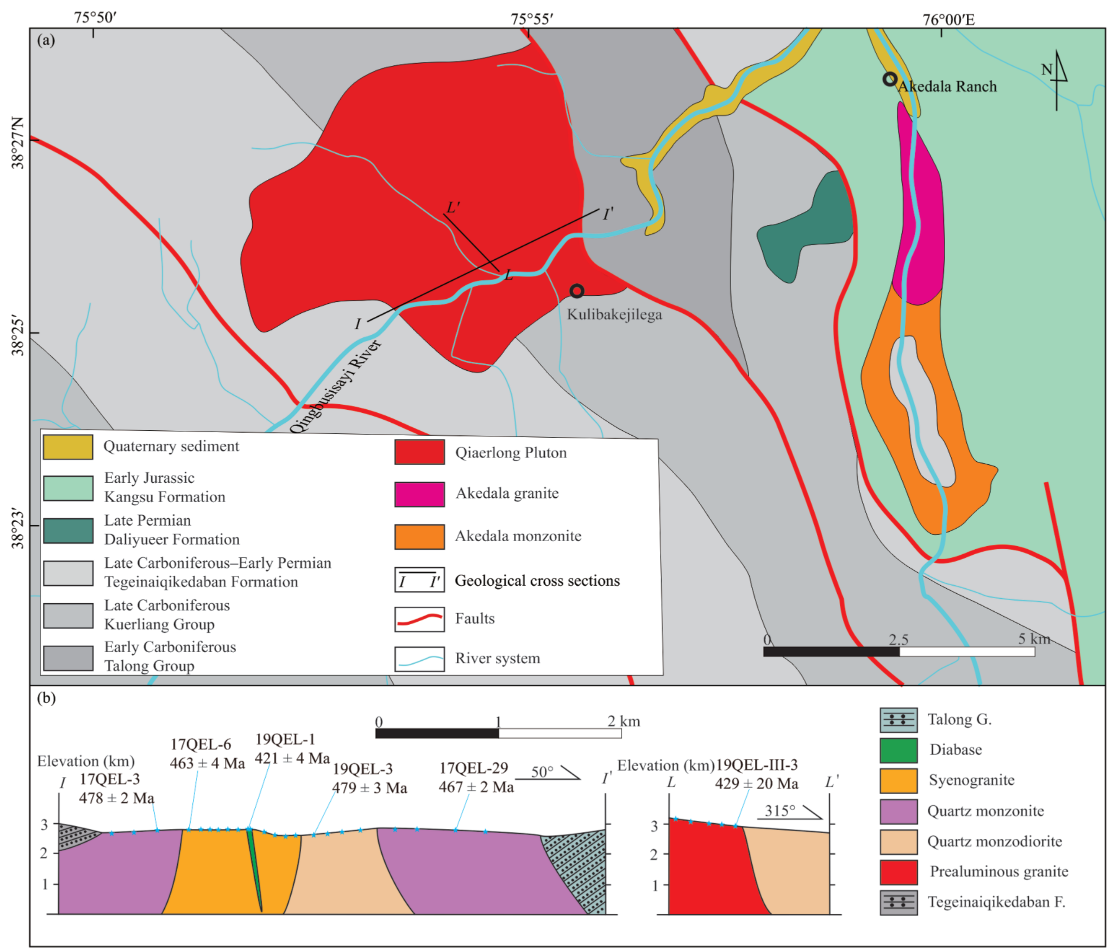

Figure 2. (a) Geological map of the Qiaerlong Pluton (modified after HIGS, 2005); (b) geological cross sections of the Qiaerlong Pluton are based on field investigation taken in 2017 and 2019.

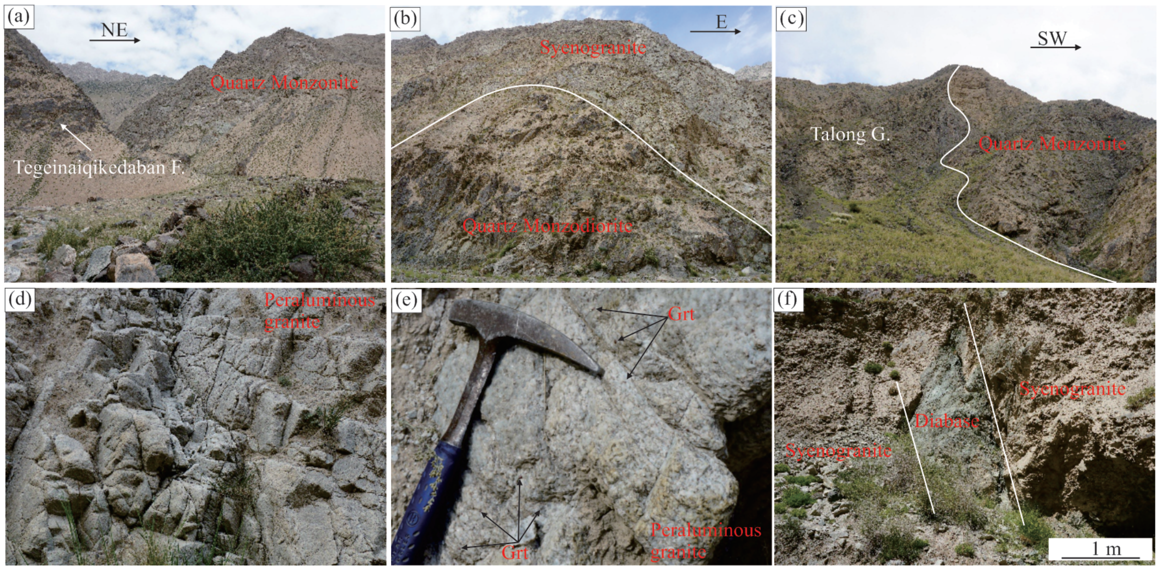

Figure 3. Photographs showing the outcrops for representative lithologies from the Qiaerlong Pluton. Grt. Garnet.

Petrographic observations reveal that quartz monzodiorites consist of hornblende (15% – 30%), plagioclase (40% – 50%), K-feldspar (10%–20%), and quartz (1%–10%) (Figure 4a); quartz monzonites consist of hornblende (10%–20%), plagioclase (40%–50%), K-feldspar (20%–30%), and quartz (1%–10%) (Figure 4b); syenogranites consist of hornblende (1% – 5%), plagioclase (10% – 20%), K-feldspar (40% – 50%), and quartz (20%–30%) (Figure 4c); and peraluminous granite consist of garnet (1% – 5%), mica (1% – 5%), plagioclase (10% – 15%), K-feldspar (30%–40%), and quartz (30%–35%) (Figure 4d). Accessory minerals in all different phases are dominated by titanite, apatite, and zircon, with minor columbite, thorite, and monazite in peraluminous granite (Figure 4d). Late-stage hydrothermal alteration is weak and represented by chloritization of hornblende and sericitization of feldspar (Figure 4). The original minerals of diabase are unrecognizable due to strong late-stage hydrothermal alteration.

2.2 Analytical Methods

We collected a total of four samples of quartz monzodiorite, seven samples of quartz monzonite, ten samples of syenogranite, six samples of peraluminous granite, and two samples of diabase from the Qiaerlong Pluton for whole-rock major and trace element analyses. Among them, six representative samples were selected for zircon and apatite U-Pb dating, including one quartz monzodiorite (19QEL-03: 38° 25′38″N, 75° 53′59″E), two quartz monzonite (17QEL-03: 38°25′28″N, 75° 53′22″E; and 17QEL-29: 38°26′00″N, 75°55′19″E), one syenogranite (17QEL-06: 38° 25′32″N, 75° 53′27″E), one peraluminous granite (19QEL-III-03: 38° 26′11″N, 75° 54′04″E), and one diabase (19QEL-01: 38°25′39″N, 75°48′57″E). All experiments were conducted at the State Key Laboratory of Ore Deposit Geochemistry, Institute of Geochemistry, at the Chinese Academy of Sciences.

Zircon and apatite were separated from each sample using traditional heavy liquid and magnetic separation techniques, handpicked under a binocular microscope, mounted with epoxy resin, and polished down to near-half sections to reveal internal structures for cathodoluminescence (CL) imaging, U-Pb dating, and Hf isotopic analyses.

Major elements were determined using an ARL Perform' X 4200 (Thermo Fisher) followed by the procedures described by Chen et al. (2012). Trace-element analyses were performed using a Perkin-Elmer Sciex ELAN DRC-e inductively coupled plasma mass spectrometer (ICP-MS) following the procedures described by Liang et al. (2000). U-Pb dating and trace-element analyses for zircon were performed using a GeoLas Pro 193 nm ArF excimer laser connected to an Agilent 7500x ICP-MS, and for apatite were performed using a GeoLas Pro 193 nm ArF excimer laser connected to an Element XR ICP-MS. Both follow the procedures described by Tang et al. (2020). Data processing was performed using ICPMSDataCal (Liu et al., 2010, 2008) and Concordia plots and weighted mean ages were derived using Isoplot (Ludwig, 2003). Zircon Lu-Hf isotope analyses were performed using a RESOlution S-155 laser ablation system (ASI, Australia) connected to a Nu Plasma III multicollector (MC) ICP-MS (Nu Instruments, Wrexham, UK) following the procedures described by Tang et al. (1998). The analytical methods and detailed procedures are given in Appendix A.

3 ANALYTICAL RESULTS

3.1 Zircon and Apatite LA-ICP-MS U-Pb Dating

The zircons separated from quartz monzodiorite, quartz monzonite, and syenogranite are 50–300 μm long with length/width ratios of 1 : 1 to 3 : 1, and are subhedral and colorless, and show well-developed oscillatory zoning without core-mantle structure in the CL images (Figures 5a–5d), indicating magmatic affinity (Hoskin and Black, 2000; Rubatto and Gebauer, 2000). La-ICP-MC analysis reveals all of zircons had high Th/U ratios of 0.6–2.8 (Table S1), further indicating magmatic affinity (Wu and Zheng, 2004; Corfu, 2003; Williams et al., 1996).

Twenty analytical spots of quartz monzodiorite sample 19QEL-03 yielded a concordant age of 479 ± 4 Ma (MSWD = 0.17, 2σ), and a weighted mean $^{206}Pb/^{238}U$ age of 479 ± 3 Ma (MSWD = 0.17, 2σ, Figure 6a). Twenty-two analytical spots of quartz monzonite sample 17QEL-03 had a concordant age of

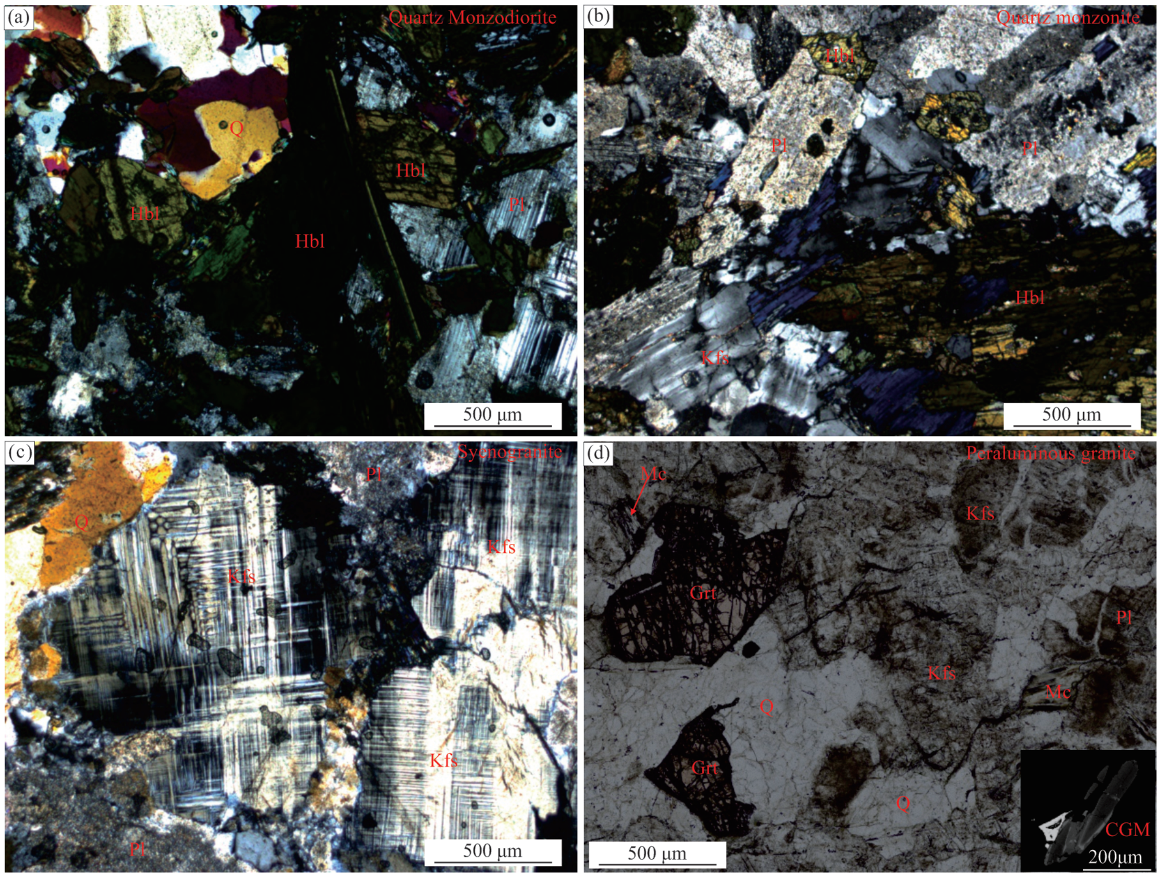

Figure 4. Photographs showing the major mineral assemblages and typical textures for representative lithologies from the Qiaerlong Pluton. Hbl. Hornblende; Kfs. K-feldspar; Pl. plagioclase; Grt. garnet; Mc. mica; Q. quartz.

478 ± 3 Ma (MSWD = 0.42, 2σ), and a weighted mean ^{206}Pb/^{238}U age of 478 ± 2 Ma (MSWD = 0.40, 2σ, Figure 6b). Twenty-three analytical spots of quartz monzonite sample 17QEL-29 had a concordant age of 467 ± 3 Ma (MSWD = 0.87, 2σ), and a weighted mean ^{206}Pb/^{238}U age of 467 ± 2 Ma (MSWD = 0.98, 2σ, Figure 6c). Eighteen analytical spots of syenogranite sample 17QEL-06 had a concordant age 463 ± 3 Ma (MSWD = 2.90, 2σ), and a weighted mean ^{206}Pb/^{238}U age of 463 ± 4 Ma (MSWD = 2.60, 2σ, Figure 6d).

The CL images and La-ICP-MC analysis suggested that there were three different types of zircons in the diabase sample 19QEL-01 (Figure 5e). Type I zircons were dark and had broad oscillatory zoning, and had a concordant age of 420 ± 5 Ma (MSWD = 0.12, 2σ) a weighted mean ^{206}Pb/^{238}U age of 421 ± 4 Ma (MSWD = 0.13, 2σ, Figure 6e), suggesting that the diabase was formed during the Middle Silurian. Type II zircons were colorless and had well-developed oscillatory zoning, and yielded a concordant age of 463 ± 5 Ma (MSWD = 0.19, 2σ), and a weighted mean ^{206}Pb/^{238}U age of 463 ± 5 Ma (MSWD = 0.17, 2σ, Figure 6e), indicating that they were captured from the host syenogranite. Type III zircons were colorless and had a core-mantle structure; the edges exhibited clear oscillatory zoning and were relatively dark, while the cores showed eroded structures with broad growth zoning and were relatively bright; 12 analytical spots for the core zircons had a concordant age of 1 059 ± 27 Ma (MSWD = 1.03, 2σ), and a weighted mean ^{207}Pb/^{206}Pb age of 1 048 ± 39 Ma (MSWD = 1.01, 2σ, Figure 6e); suggesting that they were inherited zircon.

The apatites separated from sample 19QEL-III-03 were 150–300 μm long with length/width ratios of 1 : 1 to 2 : 1. They were colorless to light-brown, irregular in shape, and uniform in the CL images (Figure 5f). All 26 analytical spots had variable U (1.27 ppm–29.4 ppm) and Th (1.81 ppm–45.2 ppm) concentrations, with high Th/U ratios of 0.3–3.1 (Table S1), and yielded a U-Pb Tera-Wasserburg concordia lower intercept age of 429 ± 20 Ma (MSWD = 1.20, 2σ, Figure 6f).

3.2 Major and Trace Elements

Major and trace element data of all the samples from the Qiaerlong Pluton are listed in Table S2. The Early Ordovician granitoids can be divided into two groups: low-K and high-K granitoids. The low-K quartz monzodiorites have SiO_2 (50.92 wt.%–56.49 wt.%), K_2O (1.03 wt.%–1.94 wt.%) and alkalis (K_2O + Na_2O = 3.98 wt.%–6.12 wt.%) values (Figures 7a–7b), and are metaluminous with A/CNK and A/NK ratios of 0.67–0.88 and 1.93–2.33 (Figure 7c), respectively. The high-K quartz monzonites and syenogranite show variation in SiO_2 (50.84 wt.%–73.33 wt.%), K_2O (2.09 wt.%–4.49 wt.%), and alkalis (K_2O + Na_2O = 6.44 wt.%–8.03 wt.%) values (Figures 7a–7b), and are metaluminous to peraluminous with A/CNK and A/NK ratios of 0.87–1.27, and 1.23–2.50 (Figure 7c), respectively.

The Middle Silurian peraluminous granites and diabases belong to high-K and low-K calc-alkaline series (Figures 7a–

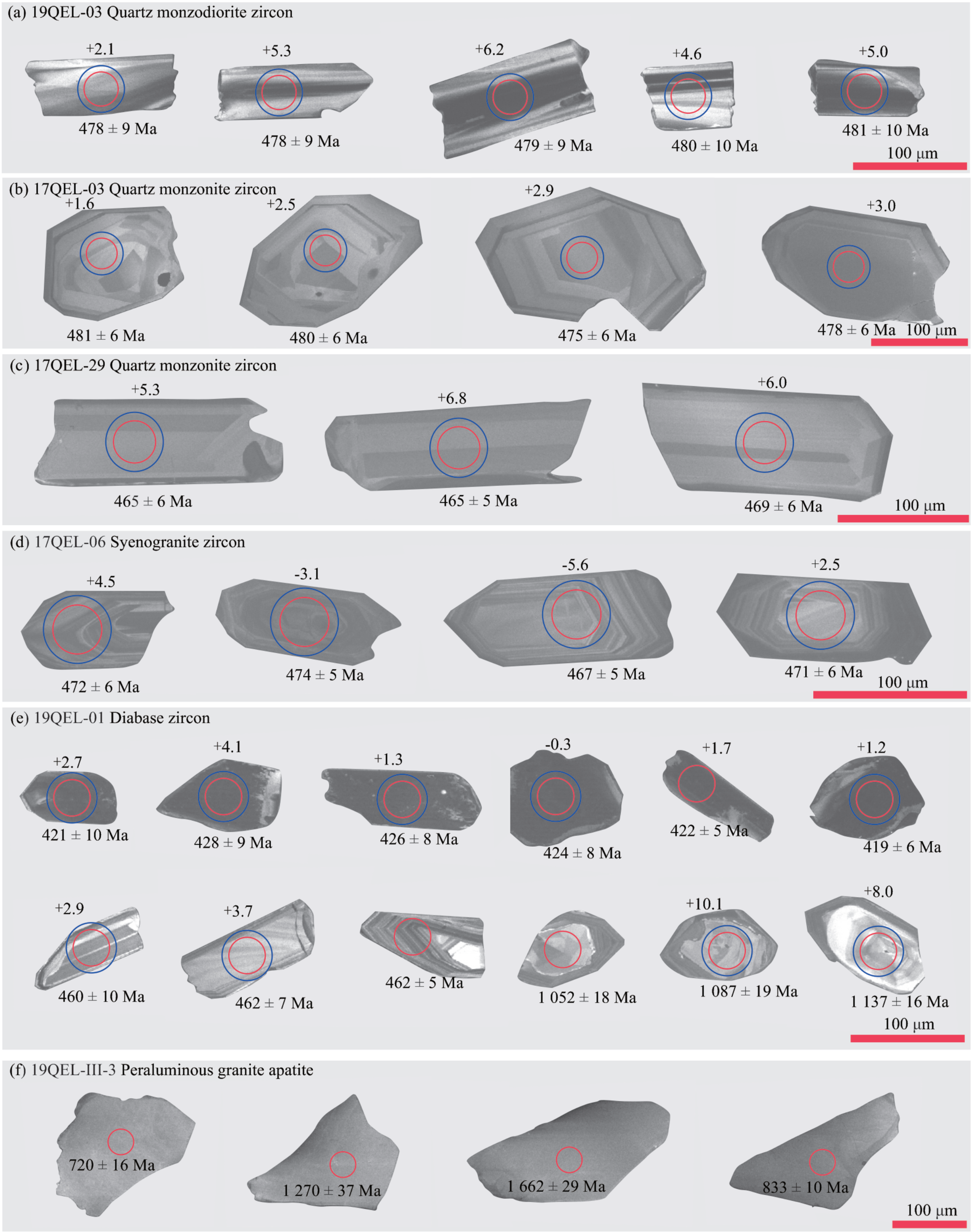

Figure 5. Representative cathodoluminescence (CL) images of zircon and apatite from the Qiaerlong Pluton. Solid red and purple circles show the location of LA-ICP-MS U-Pb analyses and LA-MC-ICP-MS Hf analyses, respectively.

7b), respectively. The former has high SiO_2 (74.92 wt.%–75.88 wt.%) and high K_2O (3.74 wt.%–4.43 wt.%), alkalis (K_2O + Na_2O = 7.97 wt.%–8.43 wt.%) contents, and is peraluminous with A/CNK and A/NK ratios of 1.15–1.22 and 1.25–1.30 (Figure 7c), respectively. The later contains low SiO_2 (53.23 wt.%–56.31 wt.%) and K_2O (1.48 wt.%–2.36 wt.%) and alkalis (K_2O + Na_2O = 5.48 wt.%–5.96 wt.%) contents, and is metaluminous with A/CNK and A/NK ratios of 0.85–1.00 and 1.98 (Figure 7c), respectively.

The Early Ordovician granitoids have variable total rare earth element (REE) of 59.7 ppm – 197 ppm, and invariably show relative enrichment of light REEs (LREEs) and have variable Eu anomalies (δEu = 0.52–1.33) in chondrite-normalized REE patterns (Figures 8a–8c), and show Rb, Ba, K, and LREE enrichment, and Nb, Ta, P, Zr, Hf, and Ti depletion in primitive mantle-normalized multi-element diagrams (Figures 8d–8f).

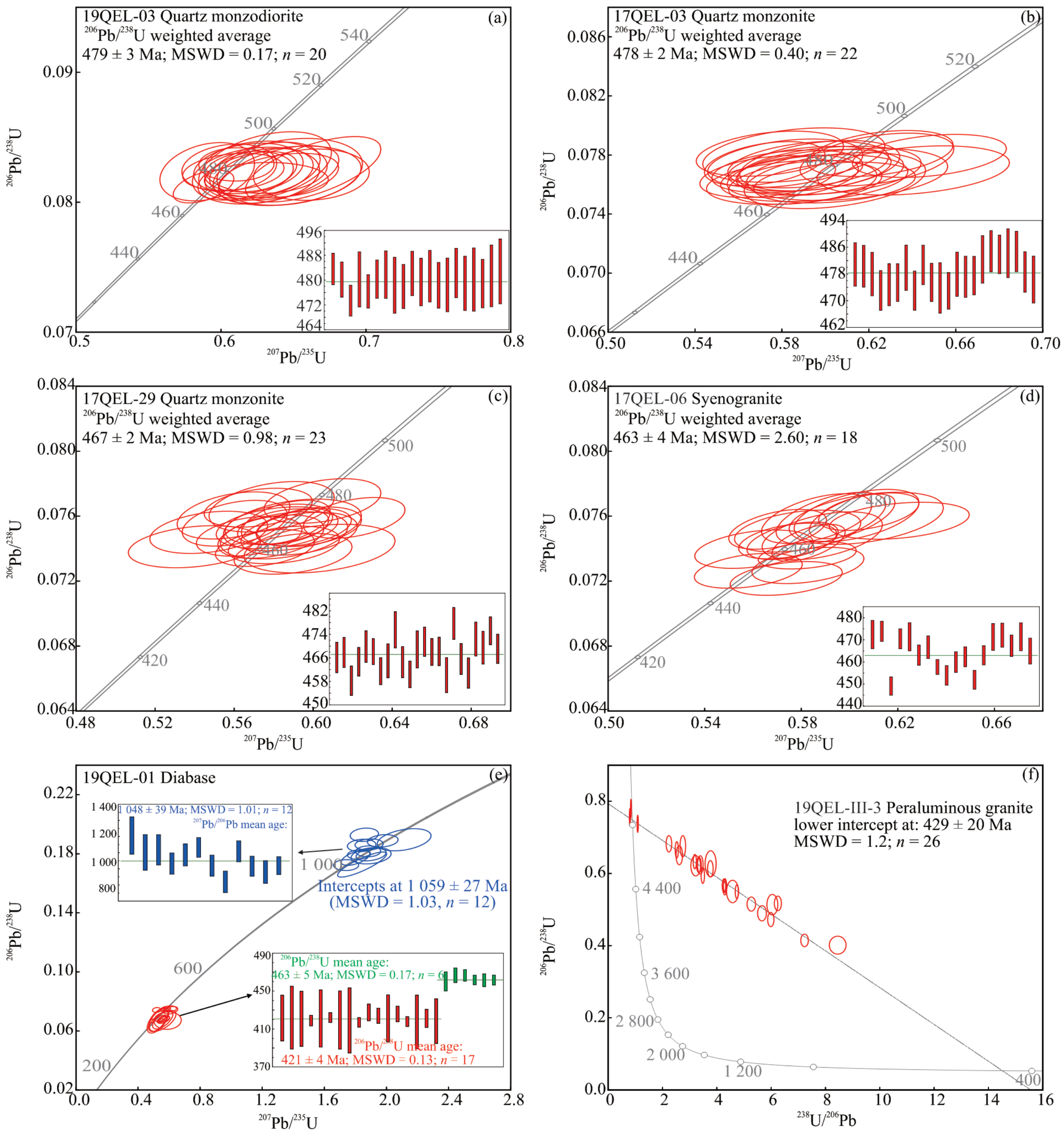

Figure 6. Age diagrams for the Qiaerlong Pluton.

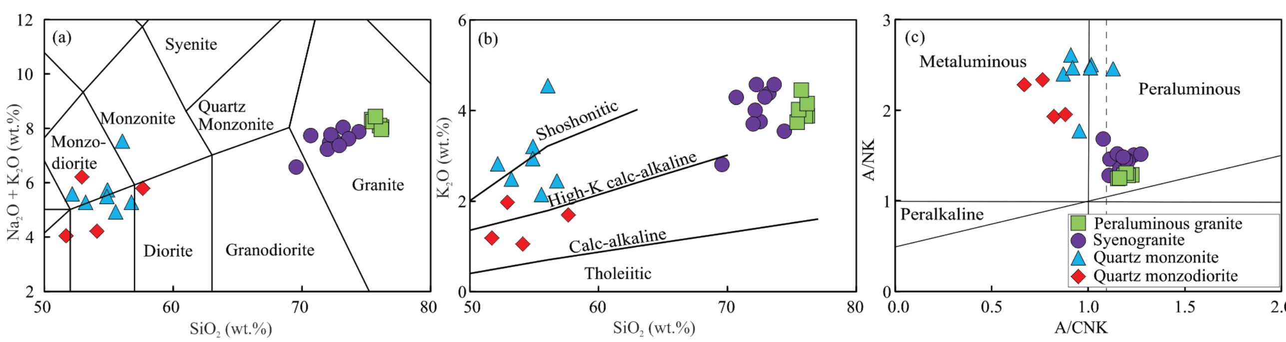

Figure 7. Classification diagrams of the Qiaerlong Pluton. (a) TAS (modified from Middlemost, 1994); (b) K_2O *vs*. SiO_2 (modified from Peccerillo and Taylor, 1976); and (c) A/NK *vs*. A/CNK (modified from Maniar and Piccoli, 1989).

The peraluminous granites have very low total REE contents of 41.5 ppm–57.9 ppm, and have remarkable negative Eu anomalies (δEu = 0.03 – 0.14), and display the tetrad effect in chondrite-normalized REE patterns (Figure 8g), and show Ba, Ta P, U, and Hf enrichment, and Nb, Sr, Zr, Hf, and Ti depletion in primitive mantle-normalized multi-element diagrams (Figure 8h). However, the diabases have high total REE content of 135 ppm – 148 ppm, and show no Eu anomalies (δEu = 1) in chondrite-normalized REE patterns (Figure 8g), and show Rb, Ba, K, and LREE enrichment, and Nb, Ta, P, Zr, Hf, and Ti depletion in primitive mantle-normalized multi-element diagrams (Figure 8h).

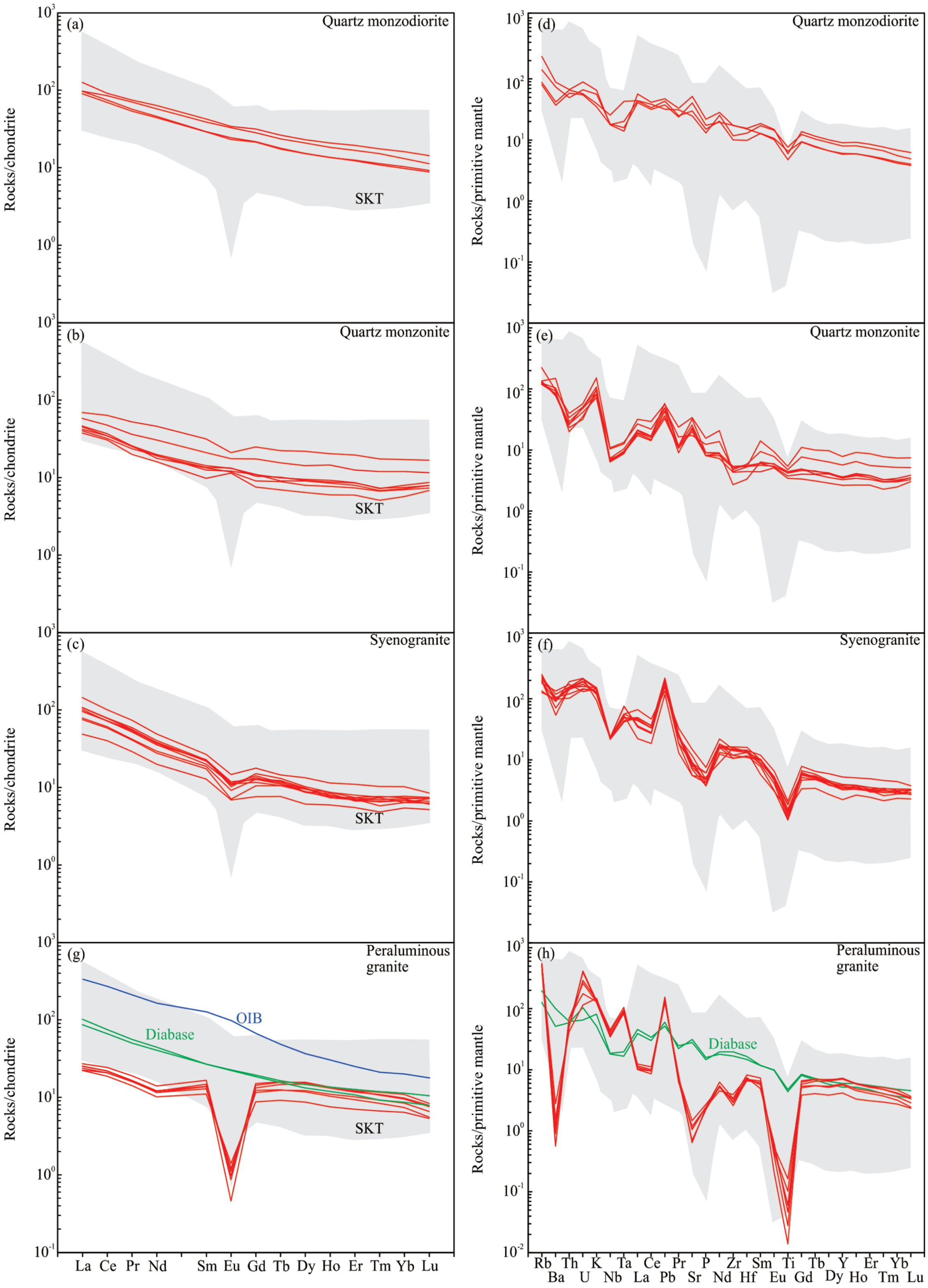

Figure 8. Chondrite-normalized REE patterns and Primitive mantle (PM)-normalized trace element patterns for the Qiaerlong Pluton. Chondrite and PM values are from Sun and McDonough (1989).

3.3 Hf Isotope Compositions of Zircon

The zircon *in-situ* Lu-Hf isotopes for the Qiaerlong Pluton were listed in Table S3 and shown in Figure 9. The quartz monzodiorite and quartz monzonite had positive zircon $\varepsilon_{Hf}(t)$ values of +0.6 to +9.9 and a two-stage Hf model age of 0.78–1.23 Ga. However, the syenogranite had variable $\varepsilon_{Hf}(t)$ values of -5.6 to +4.5 and two-stage Hf model ages of 1.07–1.63 Ga. The diabase and peraluminous granite also displayed variable $\varepsilon_{Hf}(t)$ values of -2.9 to +4.1 and two-stage Hf model ages of 1.06–1.45 Ga. But the captured zircons and inherited zircons of diabase showed positive $\varepsilon_{Hf}(t)$ values of +2.9 to +11.8.

4 DISCUSSION

4.1 Genetic Types

Granitoids are usually classified as S-, I-, and A-types (Whalen et al., 1987; Collins et al., 1982). The studied Ordovician granitoids have low-moderate SiO_2 contents (50.84 wt.%–73.33 wt.%), $(K_2O + Na_2O)/CaO$ ratios (0.51–8.53), and FeO^T/MgO ratios (1.71–2.64), suggesting that they did not experience strong separation and crystallization during formation (Figures 10a, 10d). The 10 000Ga/Al ratios (2.64–10.9) and Ga contents (22.5 ppm–105 ppm) were higher than those of A-type granites (2.6 and 20, respectively; Whalen et al., 1987), indicating A-type granite affinity (Figures 10a–10c). However, the studied rocks had lower Zr (30.1 ppm–195 ppm), Nb (4.52–18.2), and (Zr + Nb + Ce + Y) (80.6 ppm–320 ppm) values than A-type granites (250, 20, and 350, respectively; Whalen et al., 1987), indicating that the Ordovician granitoids do not belong to A-type granites (Figures 10b–10d). The petrographic observations show that the mafic minerals in the Ordovician granitoids are mainly hornblende (Figures 3–4), indicating that they have the characteristics of I-type granite (Barbarin, 1999).

The Middle Silurian peraluminous granites are characterized by low mafic minerals (Figures 3–4), suggesting that they are leucogranites (Wu and Zheng, 2014). These rocks had a high SiO_2 content (74.92 wt.%–75.88 wt.%), low Nb/Ta ratios (6.97–8.10) and Zr/Hf ratios (13.5–19.1), and were highly depleted in Ba, Sr, Ti, and Eu (Figure 8), and had high $(K_2O + Na_2O)/CaO$ ratios (14.9–27.7) and FeO^T/MgO ratios (3.63–5.22) (Figures 10a, 10d), indicating a high degree of fractionation (Wu et al., 2003; Chappell and White, 1974). Previous studies have shown that highly fractionated granite has the characteristics of A-type granite (Wu et al., 2017; Whalen et al., 1987). The peraluminous granites had higher 10 000Ga/Al (2.71–3.09) ratios and Ga (20.4–23.2) and Nb (24.4 ppm–31.6 ppm) values than those of A-type granites (2.6, 20 and 20, respectively; Whalen et al., 1987), suggesting an A-type granite affinity (Figures 10a–10c). However, the Zr (28.9 ppm–43.9 ppm) and (Zr + Nb + Ce + Y) (100 ppm–118 ppm) contents of these rocks were distinct from those of A-type granites (Figures 10b–10d; Whalen et al., 1987). The peraluminous granites had similar A/CNK ratios (1.15–1.22) to S-type granite (Chappell and White, 1974), and had peraluminous minerals (i. e., garnet and mica; Figures 4–5), indicative of S-type granite affinity (Barbarin, 1999). However, their zircon $\varepsilon_{Hf}(t)$ values (-2.9 to +2.0) were higher than S-type granite (< -6; Kemp et al., 2007).

Experimental studies have shown that the solubility of apatite in metaluminous to weakly peraluminous magma systems is very low and decreases with increasing SiO_2 content along with crystallization differentiation; however, solubility increases with the increase in SiO_2 in strongly peraluminous systems (Wu et al., 2003; Chappell and White, 1974). The Qiaerlong Pluton has variable A/CNK ratios (0.67–1.27), suggesting metaluminous to peraluminous conditions. The P_2O_5 content decreases with increasing SiO_2 content in all the studied rocks (Figure 10e), which is consistent with the trend for I-type granites (Wu et al., 2003; Chappell and White, 1992). Previous studies have revealed that Y-rich minerals will crystallize in the late stage of metaluminous I-type magma; therefore, the Y content increases with increasing SiO_2 content, and has a positive correlation with Rb content (Li et al., 2007). The Y *vs*. Rb diagram for the Qiaerlong Pluton (Figure 10e) also suggests a trend comparable to I-type granite.

Moreover, magmatic temperatures are useful to diagnose genetic types of granitoids (Luo et al., 2020; Zhai et al., 2020; Qin et al., 2019; King et al., 1997), and is generally calculated and whole-rock zircon saturation thermometers (Watson and Harrison, 1983). The calculated whole-rock zircon saturation temperatures of quartz monzodiorite, quartz monzonite, syenogranite, and peraluminous granite of Qiaerlong Pluton are 667–754 °C (mean 709 °C), 617–688 °C (mean 657 °C), 767–813 °C (mean 790 °C), and 670–695 °C (mean 682 °C) (Table S2), respectively. These temperatures are similar to the average value

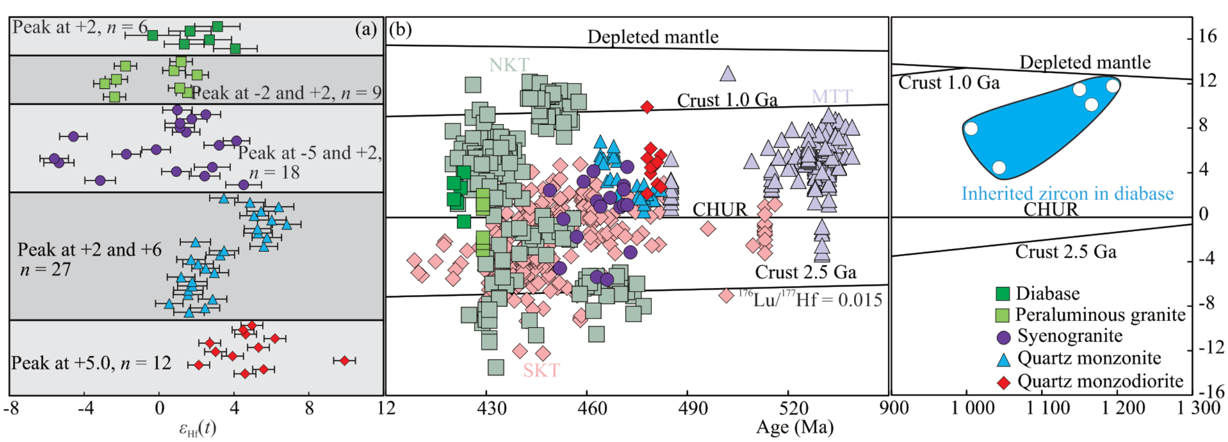

Figure 9. (a) Initial zircon $\varepsilon_{Hf}(t)$ values for the Qiaerlong Pluton (modified from Wang et al., 2014); (b) $\varepsilon_{Hf}(t)$ values *vs*. zircon U-Pb ages for the Qiaerlong Pluton.

of fractionated I-type granite (760 °C), but are obviously lower than the average value of for A-type granites (840 °C; King et al., 1997), further suggesting that they belonged to I-type granite.

Overall, although the Qiaerlong Pluton shows similarities with S-type and A-type granites, the overall characteristics of the rocks indicate that the pluton should be classified as I-type granite.

4.2 Petrogenesis

The Early Ordovician granitoids had variable SiO_2 contents (50.84 wt.%–73.33 wt.%) and had high $Mg^{\#}$ (40–51) values, suggesting that they were derived from a mixed mafic and felsic source. The peraluminous granites were highly fractionated and, therefore, their major and trace elements do not reflect the characteristics of the magma source. However, zircon Hf isotopes show great potential in this regard (Griffin et al., 2002).

The zircon $\varepsilon_{Hf}(t)$ values varied by at least 5 ε_{Hf} units for all studied rocks, with values of +2.1 to +9.9 for quartz monzodiorites, +0.6 to +6.8 for quartz monzonites, -5.6 to +4.5 for syenogranites, and -2.9 to +2.0 for peraluminous granites, indicating that all of them were originated from mixed sources (Figure 9a; Griffin et al., 2002).

The positive zircon $\varepsilon_{Hf}(t)$ values of quartz monzodiorites and quartz monzonites (+0.6 to +9.9) plotted above the CHUR reference line (Figure 9b), and two-stage Hf model ages (0.78–1.23 Ga) of them were comparable to the crystallization age (920–1 207 Ma) of inherited zircon in the diabase (Table S2), suggesting that they were derived from a mixed source of juve-

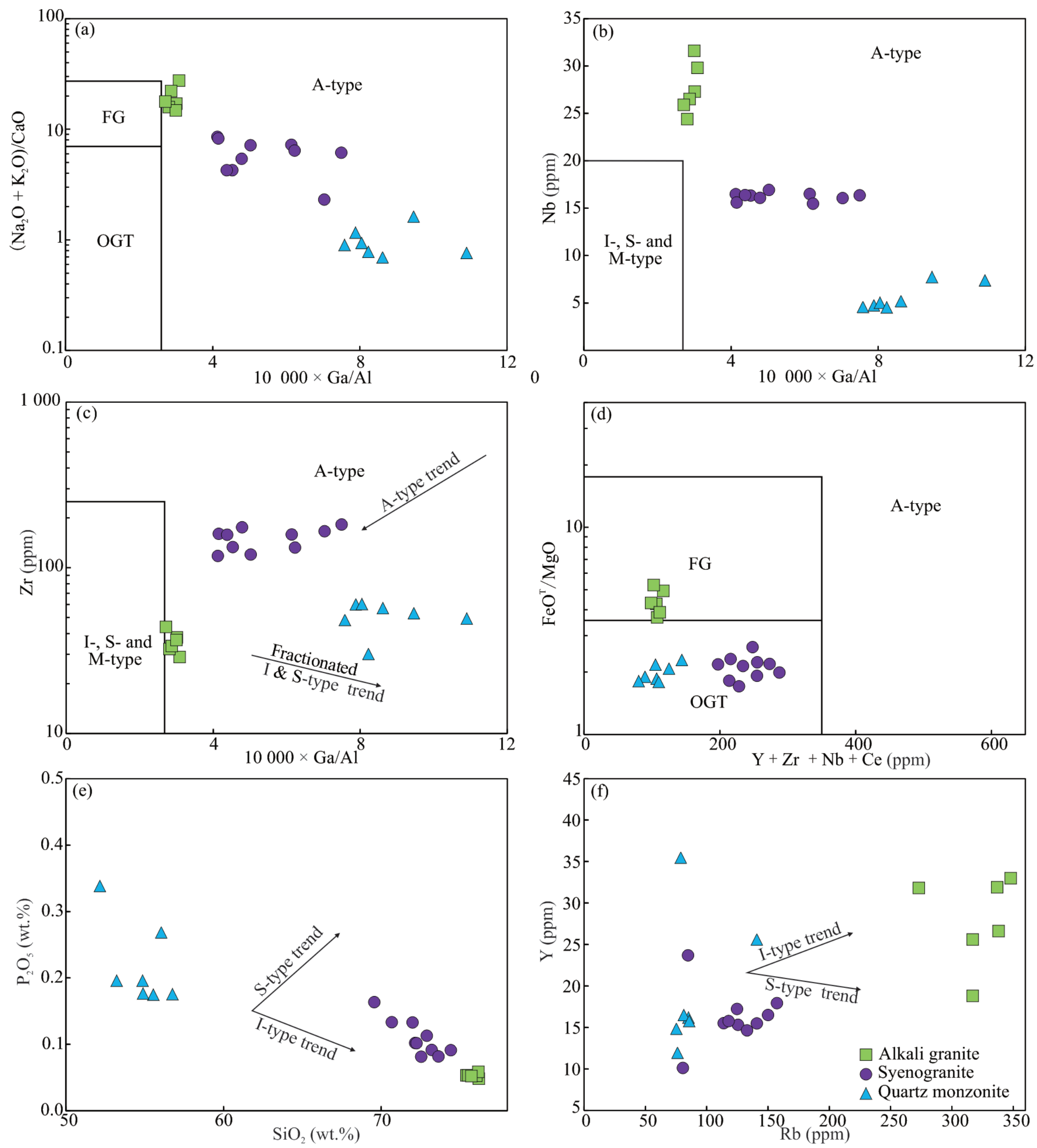

Figure 10. Discrimination diagrams for the Qiaerlong Pluton ($Na_2O + K_2O/CaO$) *vs.* 10 000 × Ga/Al (a); Nb *vs.* 10 000 × Ga/Al (b); Zr *vs.* 10 000 × Ga/Al (c); FeO^T/MgO *vs.* Y + Zr + Nb + Ce (d); P_2O_5 *vs.* SiO_2 (e); Y *vs.* Rb (f). I. I-type granitoids; S. S-type granitoids; M. M-type granitoids; A. A-type granitoids; FG. fractionated granitoids; OGT. unfractionated granitoids.

nile and lower crust. The syenogranites and peraluminous granites had variable zircon $\varepsilon_{Hf}(t)$ values (-5.6 to +4.5) that plotted on both sides of the CHUR reference line in the t-$\varepsilon_{Hf}(t)$ diagram (Figure 9b), indicating that they were derived from a mixing of partial melting of older and upper crust.

The diabase had high SiO_2 (53.23 wt.%–56.31 wt.%) contents, low $Fe_2O_3^T$ (7.59 – 7.91), and MgO (3.48 wt.% – 4.61 wt.%), and $Mg^\#$ (48 – 54) values (Table S2), and had variable zircon $\varepsilon_{Hf}(t)$ values of -0.3 to +4.1 (Table S3), and displayed the characteristics of arc magma (Figures 8g – 8h), suggesting that they were sourced from a depleted mantle, and underwent crustal contamination and crystallization (Münker et al., 2003; Saunders et al., 1992).

The diabase had Nb/La ratios ranging from 0.42 to 0.48 that were comparable to the Nb/La ratios of subcontinent lithospheric mantle (SCLM) melt (< 1; DePaolo and Daley, 2000), indicating a SCLM origin. The flat chondrite-normalized REE patterns of the diabase revealed hornblende residues that are stable in SCLM (Class and Goldstein, 1997), further suggesting a SCLM origin. They had similar Nb/U (5.89–9.71) ratios to continental crust (6.15; Rudnick and Gao, 2003), and contained captured zircon and inherited zircon (Figures 5–6), demonstrating that the diabase experienced crustal contamination during emplacement. Fractionation of hornblende results in low Nb/Ta and high Zr/Hf ratios because it has D(Nb/Ta) > 1 and D(Zr/Hf) < 1 (Foley et al., 2001; Tiepolo et al., 2001). The studied diabase has subchondritic Nb/Ta ratios (16.5–18.9) (19.9; Münker et al., 2003) and superchondritic Zr/Hf ratios (41.3 – 43.1) (34.3; Münker et al., 2003), revealing hornblende fractionation.

The diabase had high Ba/Th (71.4–135) and U/Th (0.26–0.44) ratios, and low Th/Ce (0.086 – 0.094) and Th/Nb (0.38 – 0.39) ratios, indicating that its source (SCLM) has been metasomatized by subducted fluids (Hawkesworth et al., 1997). This metasomatism may be ascribed to the subduction of the Proto-Tethys oceanic slab.

The Ordovician granitoids are enriched in LILEs (i.e., Rb, Ba, and LREEs) and depleted in HFSEs (i.e., Nb, Ta, P, Zr, Hf, and Ti), suggesting that they were formed under a subduction environment and that subducted sediments or fluids may have participated in the diagenesis process (Martin et al., 2005; Hawkesworth et al., 1997). Previous studies have revealed that subducted sediments were involved in the formation of the Datong Complex (Liu et al., 2014; Liao et al., 2010). The Ordovician granitoids had much higher Ba/Nb ratios (16.0–229) than MORB (6.9; Sun and McDonough, 1989) and much lower Nb/U (3.6–15.2) and Ta/U (0.3–1.5) ratios than MORB (46.1 and 2.6, respectively; Sun and McDonough, 1989), indicating the contribution of subducted fluids (Wang and Xiao, 2018; Plank and Langmuir, 1998; Hawkesworth et al., 1997; Brenan et al., 1995; McCulloch and Gamble, 1991; Tatsumi et al., 1986). In addition, petrographic observations revealed that mafic minerals in the Ordovician granitoids are dominated by hornblende (Figures 3–4), which further implies a hydrous magma source conducive to the preferential crystallization of hornblende (Sisson et al., 1996).

The Qiarerlong Pluton underwent variable crystallization fractionation (Figure 10), which is consistent with the trends of decreasing TiO_2, $Fe_2O_3^T$, and MgO with increasing SiO_2 content (Figure 11). These negative trends are likely the result of the fractionation of mafic minerals (i.e., pyroxene, and hornblende). A positive correlation between Dy and Er in the studied pluton strongly suggests hornblende fractionation (Figure 12a), which is compatible with petrographic observations (Figures 3 – 4). This pluton had variable Eu, Ba, Sr, P, and Ti anomalies in the chondrite-normalized REE patterns and the primitive mantle-normalized multi-element diagrams (Figure 8), indicating the fractionation of plagioclase, apatite, and Fe-Ti oxides. Correlations between Rb/Sr and Sr, Sr and Eu*, Ba and Sr, and Ba and Rb also indicate the crystallization of plagioclase, K-feldspar, and hornblende (Figures 12b – 12e). The Qiarerlong Pluton has variable REE contents that are controlled by REE-enriched accessory minerals (i. e., zircon, apatite, monazite, and allanite). Correlations between La and $(La/Yb)_N$ (Figure 12f) suggest the fractional crystallization of monazite and/or allanite.

Zr/Hf and Nb/Ta ratios are usually invariant during partial melting and fractional crystallization processes (Sun and McDonough, 1989). However, research shows that the low Zr/Hf and Nb/Ta ratios varied in magma that experienced extreme Ti-rich mineral fractional crystallization (Münker et al., 2003), or that was interactive with water (Nb/Ta < 5; Ballouard et al., 2016). The Middle Silurian peraluminous granites are highly fractionated (Figures 8, 10a, 10d) and have low Zr/Hf (13.5 – 19.1) and Nb/Ta (6.97–8.10) ratios indicative of a high degree of crystal fractionation (Yang et al., 2012; Wu et al., 2003). With extreme magmatic fractionation, zircon and columbite are conducive to preferential crystallization over hafnon and tantalite, which leads to the fractionation of Zr and Hf, and Nb and Ta (Linnen and Keppler, 2002, 1997). Garnet crystallization preferentially incorporates Zr over Hf (Yin et al., 2013; Linnen and Keppler, 2002), and mica crystallization preferentially partitions Nb over Ta at low temperatures (Stepanov et al., 2014; Linnen and Keppler, 1997). The petrographic observations revealed that the peraluminous granites contained garnet, biotite, and columbite-group minerals (Figures 3 – 4), suggesting that their minerals crystal fractionation was responsible for the low Zr/Hf and Nb/Ta ratios.

In summary, field and petrographic observations, geochronology, geochemistry, and zircon Hf isotopic compositions point to complex petrogenesis where a mixture of multiple sources magma (metasomatized SCLM, juvenile, old lower, and upper crust), and contamination coupled with subsequent variable crystal fractionation was responsible for the generation of the Qiarerlong Pluton.

4.3 Tectonic Implications

Previous studies have shown that voluminous Cambrian–Ordovician magmatic rocks are widely exposed at the southeastern margin of the WKOB (Figure 1b) but are less clear at the northwestern margin because of widely developed Jurassic–Cretaceous molasses (Robinson et al., 2004) and the Late Paleozoic back-arc sedimentary basin (Zhang Z W et al., 2019, 2014; Ji et al., 2018; Zhang C L et al., 2018b, 2006; Jiang et al., 2008). Our new data suggest that the Qiaerlong Pluton crystallized during the Early Paleozoic (Figure 6). These ages indicate that this pluton was an Early Paleozoic complex at the northwestern margin of the WKOB. This is consistent with the age

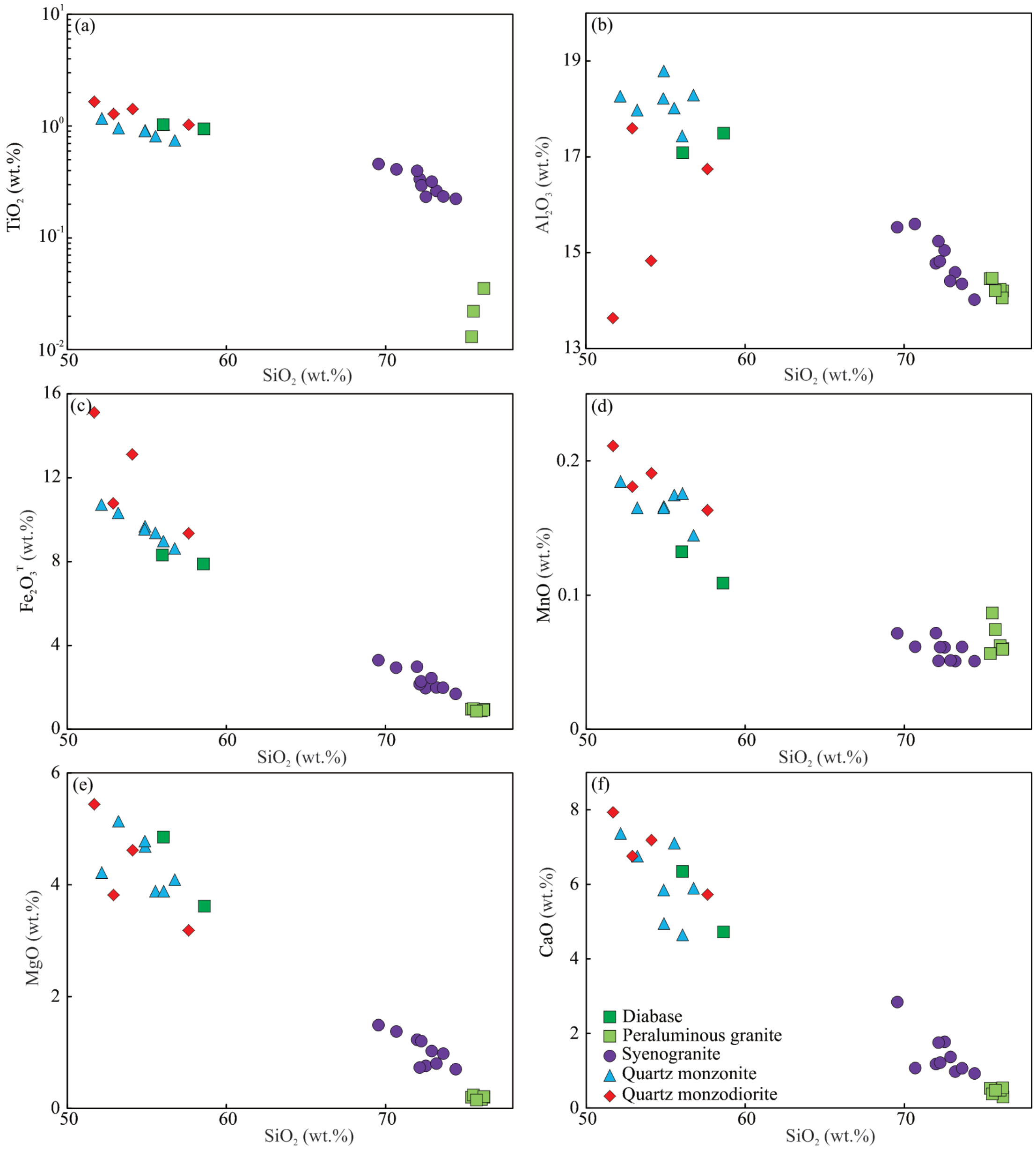

Figure 11. Selected major elements *vs*. SiO_2 diagrams for the Qiaerlong Pluton. (a) TiO_2; (b) Al_2O_3; (c) $Fe_2O_3^T$; (d) MnO; (e) MgO; (f) CaO.

of the Datong Complex (435–473 Ma; Li et al., 2019; Zhu et al., 2018; Wang et al., 2017; Jia et al., 2013; Liao et al., 2010) located in the south of the studied pluton, suggesting that the formation of the Qiaerlong Pluton was related to the tectonic evolution of the Proto-Tethys Ocean.

However, the specific dynamic links between this pluton and this subduction require further study as the location and subduction polarity of the ocean remain controversial in this area. Previous studies have proposed three contradictory models. Some researchers considered that the Proto-Tethys Ocean opened between the SKT and the MTT, and its northward and/or bidirectional subduction produced an Andean-type active continental margin and a back-arc basin with Kudi-Qimanyute ophiolite as a remnant (Yin et al., 2020; Zhang Q C et al., 2019a, b; Hu J et al., 2017; Ye et al., 2008; Xiao et al., 2005, 2000; Yuan et al., 2005; Wang, 2004; Wang et al., 2003, 2002). In contrast, some have suggested that there were two oceans between the north and south sides of the SKT, both being simultaneously subducted beneath the SKT (Wang et al., 2017, 2006). In addition, it has been suggested that the Proto-Tethys Ocean existed between the MTT and the NKT, and southward subduction beneath the MTT produced an accretionary wedge (SKT) on the north side of the MTT (Li et al., 2019; Liu et al., 2019, 2014; Zhang et al., 2019a, 2018b, c; Jia et al., 2013; Liao et al., 2010; Jiang et al., 2002).

These three models also provide different interpretations of the attributes for the SKT. It is generally believed that the Saitula Group was the basement of the SKT but recent research has shown that this group was deposited during the Early Paleozoic (Zhang et al., 2019a, b; 2018b) and the SKT was an Early Paleozoic large accretionary wedge during the southward subduction of the Proto-Tethys Ocean (Zhang et al., 2019a, b, 2018b; Xiao et al., 2005; Yuan et al., 2005). And the Early Paleozoic granitoids in this terrane lack ancient basement infor-

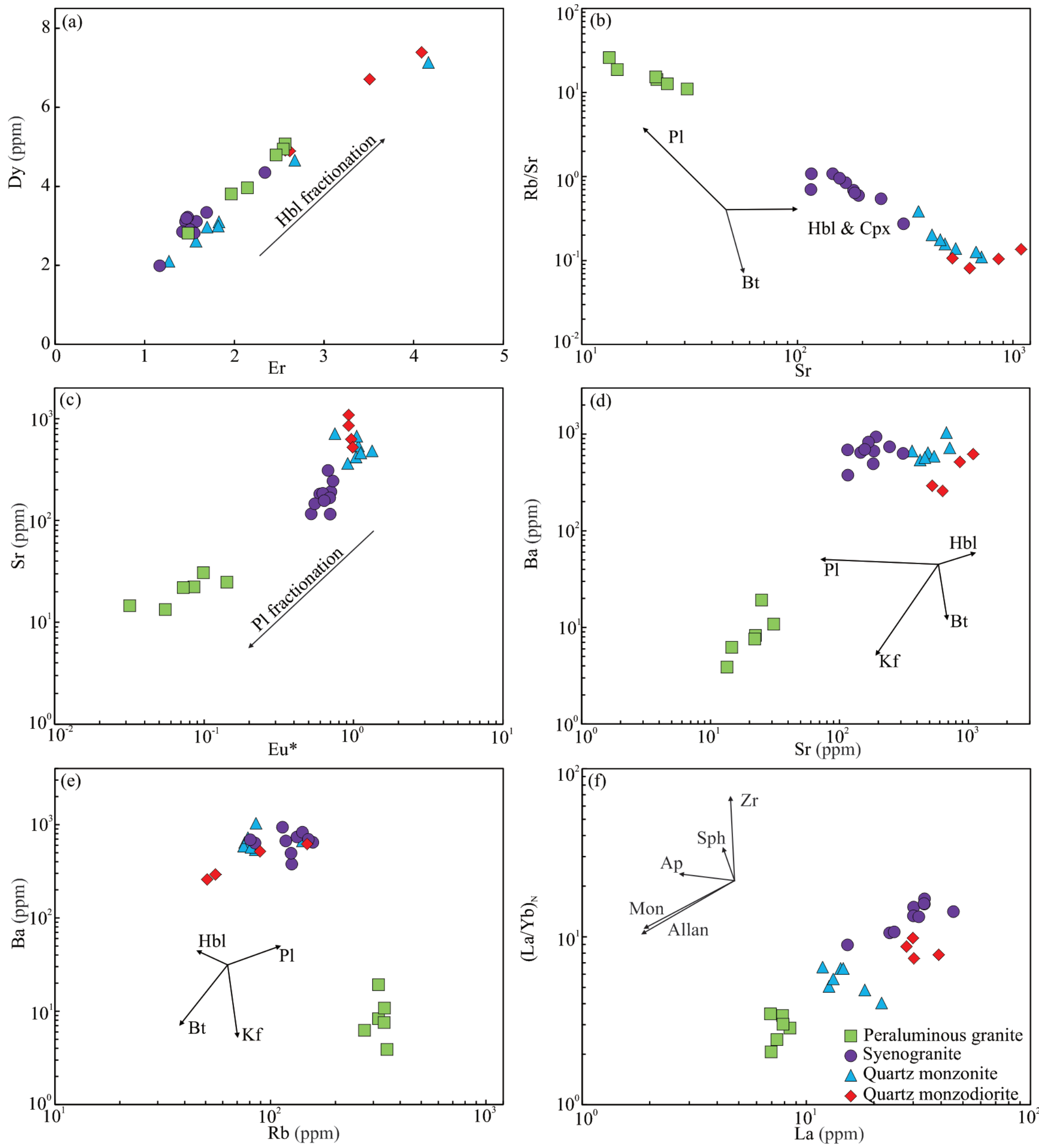

Figure 12. (a) Dy *vs*. Er diagrams showing evidence of fractionation of hornblende; (b) Rb/Sr *vs*. Sr diagrams showing evidence of fractionation of hornblende and plagioclase; (c) Sr *vs*. Eu* diagrams showing evidence of fractionation of plagioclase; (d) Ba *vs*. Sr diagrams showing evidence of fractionation of hornblende, plagioclase and K-feldspar; (e) Ba *vs*. Rb diagrams showing evidence of fractionation of K-feldspar; and (f) $(La/Yb)_N$ *vs*. La diagrams showing evidence of fractionation of monzonite and/or allanite.

mation (Yuan et al., 2003) and lack inherited zircon (Jia et al., 2013). However, these granitoids generally show two-stage Nd-Hf model ages of 1.12 to 2.51 Ga, indicating a contribution of Middle-Paleoproterozoic crust (Li et al., 2019; Zhu et al., 2018; Wang et al., 2017; Liu et al., 2014; Jia et al., 2013; Liao et al., 2010). These model ages are distinct from the crystallization age of the basement of the Tarim Basin (the Paleoproterozoic Heluositan Complex and the 2.41 Ga Akazi Pluton; Zhang C L et al., 2007) and the MTT (the 2.5 Ga Mazar Complex; Zhang et al., 2018a; Ji et al., 2011), suggesting that the SKT may have a different crystallization basement. In addition, the studied intrusion includes both mantle-derived diabase, intermediate-acid crust-derived rocks, and 1.0 Ga-inherited zircons (Figures 6, 9), indicating that these rocks are controlled by the SKT basement material.

It is generally believed that the CCOB was the result of the closure of the Proto-Tethys Ocean, with the Tarim and North China Craton to the north, and the West Kunlun, Karakunlun, Qinling, and Qaidam Blocks to the south (Figure 1a; Wu et al., 2020). The Kudi Ophiolite Suite contains the Late Cambrian to Early Ordovician ultramafic body, volcanic rock, and flysch (Li and Zhang, 2014, and references therein), and has the characteristics of a forearc, and is considered as the remnant of the Proto-Tethys Ocean in the WKOB (Li and Zhang, 2014, Xiao et al., 2005; Yuan et al., 2005; and references therein). There is currently no report of Early Paleozoic ophiolite in the MTT, suggesting that the Proto-Tethys Ocean existed between the Tarim and the SKT. The Early Paleozoic magmatic rocks mostly occur in the SKT and the MTT, with some in the NKT (Figure 1b), indicating bidirectional subduction of the Proto-Tethys oceanic slab.

The Qiaerlong Pluton is located at the northwestern margin of SKT and its Ordovician granitoids show similar geochemical characteristics to the voluminous Cambrian–Ordovician magmatic rocks in the WKOB, enriched in LILEs and depleted in HFSEs (Figure 8; Li et al., 2019; Liu et al., 2019; Zhang C L et al., 2019a, b, 2018a; Zhang Q C et al., 2019b; Zhu et al., 2018; Wang et al., 2017; Hu et al., 2016; Liu et al., 2014; Liao et al., 2010; Cui et al., 2007a, b; Xiao et al., 2005; Yuan et al., 2005), indicating that they are related to the subduction of the Proto-Tethys oceanic slab (Martin et al., 2005; Hawkesworth et al., 1997), and had low Nb, Y, and Rb values that plotted into the VAG area of the discrimination diagrams (Figure 12; Pearce et al., 1984), suggesting that the Ordovician granitoids were formed during the southward subduction of the Proto-Tethys oceanic slab. In addition, the zircon $\varepsilon_{Hf}(t)$ values of the Ordovician granitoids are similar to the Cambrian–Ordovician rocks in the SKT, but are different from NKT and MTT (Figure 9; Li et al., 2019; Liu et al., 2019; Zhang C L et al., 2019a, b, 2018a; Zhang Q C et al., 2019d; Zhu et al., 2018; Wang et al., 2017; Hu et al., 2016; Liu et al., 2014; Liao et al., 2010; Cui et al., 2007a, b; Xiao et al., 2005; Yuan et al., 2005), further indicating that the Qiaerlong pulton were related to the southward subduction of the Proto-Tethys oceanic slab.

Previous studies reported a peak metamorphic age of 450 Ma, suggesting the subduction likely continued until Late Ordovician (Zhang C L et al., 2019a, b; Ye et al., 2008; Wang, 2008; Xiao et al., 2005). The leucogranites are usually formed after peak collision and are the products of the post-orogenic stage (Wu et al., 2015; Chung et al., 2005).

Based on our observations, Middle Silurian peraluminous granites (429 Ma) have lithofacies characteristic of leucogranites (Figures 3–4) and are highly differentiated granite in geochemistry (Figure 10), suggesting that they are associated with collision. Their high Nb, Y, and Rb values plot in the post-COLG field of discrimination diagrams (Figure 13; Pearce et al., 1984), indicating that the Proto-Tethys oceanic slab had been closed during Middle Silurian. The studied diabase had a weighted mean $^{206}Pb/^{238}U$ age of 421 ± 4 Ma (Figure 6e), which is consistent with the age of north Kudi A-type granite (404–420 Ma; Liu et al., 2014; Xiao et al., 2005; Yuan et al., 2002) and Duweituwei diabase (408.5 ± 7.3 Ma; Liu et al., 2016), further suggesting a Middle Silurian post-Orogenic extension of the WKOB.

On the basis of our petrological, geochronological, and geochemical data together with the temporal and spatial characteristics of the Early Paleozoic magmatic rocks in the WKOB (Figure 1b), we propose an integrated model for the tectonic evolution of the Proto-Tethys Ocean and the studied pluton (Figure 14). The Proto-Tethys Ocean was opened between the West Kunlun Terrane and Tarim Block during break-up of the Rodinia supercontinent (Zhang C L et al., 2019a; Metcalfe et al., 2017), and initial subduction began before 530 Ma (Yin et al., 2020; Zhang C L et al., 2018c), and bidirection-

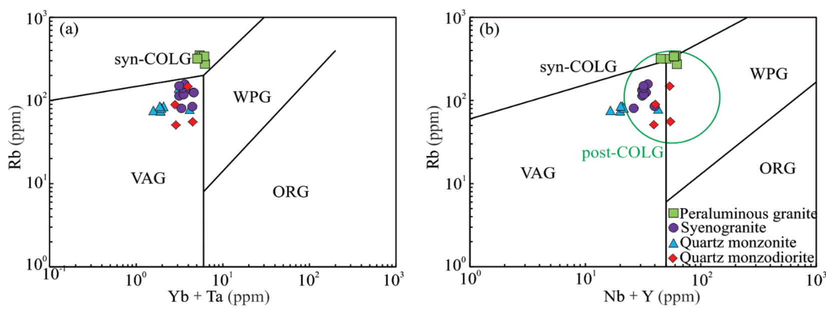

Figure 13. Discrimination diagrams for the Qiaerlong Pluton (modified from Pearce et al., 1984). Rb *vs*. Yb + Ta (a); Rb *vs*. Nb + Y (b).

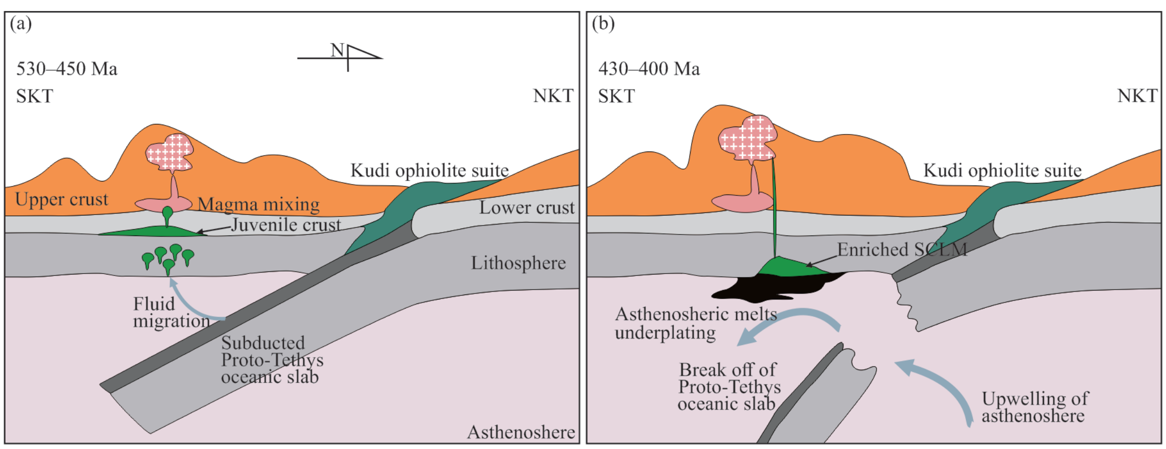

Figure 14. Tectonic model for generation of the Qiaerlong Pluton. (a) Subduction of the Proto-Tethyan Ocean occurred during 530–460 Ma, forming the Ordovician granitoids; (b) closure and slab break-off of the Proto-Tethys Ocean occurred during 450–430 Ma, forming the Middle Silurian peraluminous granites and diabase.

al subduction then continued until the Late Ordovician. The southward subduction led to the formation of the studied Ordovician granitoids (Figure 14a). Early Silurian (456 – 440 Ma) closure of the ocean led to collisions between the West Kunlun Terrane and Tarim Blocks, and which in turn caused hornblende-facies to granulite-facies metamorphism (Zhang C L et al., 2019a, b, 2018b; Wang, 2008; Xiao et al., 2005). The Middle Silurian post-Orogenic extension may have been triggered by the break-off of the Proto-Tethys oceanic slab (Zhang et al., 2019c, 2016d; Zhu et al., 2018; Jia et al., 2013; Ye et al., 2008), resulting in the emplacement of the studied peraluminous and diabase (Figure 14b).

5 CONCLUSIONS

(1) LA-ICP-MS zircon U-Pb dating reveals that Qiaerlong Pluton is composed of 479 ± 3 Ma quartz monzodiorite, 467–472 Ma quartz monzonite, 463 ± 4 Ma syenogranite, 429 ± 20 Ma peraluminous granite, and 421 ± 4 Ma diabase.

(2) Quartz monzodiorite and quartz monzonite were likely derived from a mixed source of juvenile crust and old lower crust, while syenogranite and peraluminous granite were likely generated by a mix source of old lower and upper crust. Diabase was derived from partial melting of metasomatized SCLM and experienced crustal contamination.

(3) Variable crystal fractionation was responsible for the generation of the Qiarerlong Pluton.

(4) The Ordovician granitoids were ascribed to southward subduction of the Proto-Tethys Ocean, and the Middle Silurian diabase and highly fractionated peraluminous granite (leucogranite) were mostly likely associated with slab break-off of the Proto-Tethys Ocean.

ACKNOWLEDGMENTS

This contribution was financially supported by the Natural Science Foundation of China (NSFC Nos. U1603245, 41703051, U1812402), the Chinese Academy of Sciences “Light of West China” Program, and the Natural Science Foundation of Guizhou Province (No. [2018]1171). The authors thank Mr. Guangbing Ding and Mr. Hongjun Qin for fieldwork assistance, and are grateful to Dr. Yanwen Tang (U-Pb dating), Ms. Shuqing Yang (whole-rock major element), Ms. Jing Hu and Ms. Yan Huang (whole-rock trace element), Dr. Youwei Chen (Hf isotope), and Ms. Shaohua Dong (Cathodoluminescence) for experiment analysis. The final publication is available at Springer via https://doi.org/10.1007/s12583-021-1453-8.

Electronic Supplementary Materials: Supplementary materials (Tables S1, S2, S3; Appendix A) are available in the online version of this article at https://doi. org/10.1007/s12583-021-1453-8.

Conflict of Interest

The authors declare that they have no conflict of interest.

REFERENCES CITED

Ballouard, C., Poujol, M., Boulvais, P., et al., 2016. Nb-Ta Fractionation in Peraluminous Granites: A Marker of the Magmatic-Hydrothermal Transition. *Geology*, 44(3): 231–234. https://doi.org/10.1130/g37475.1

Barbarin, B., 1999. A Review of the Relationships between Granitoid Types, Their Origins and Their Geodynamic Environments. *Lithos*, 46(3): 605–626. https://doi.org/10.1016/s0024-4937(98)00085-1

Brenan, J. M., Shaw, H. F., Ryerson, F. J., 1995. Experimental Evidence for the Origin of Lead Enrichment in Convergent-Margin Magmas. *Nature*, 378(6552): 54–56. https://doi.org/10.1038/378054a0

Chappell, B. W., White, A. J. R., 1974. Two Contrasting Granite Types. *Pacific Geology*, 8: 173–174

Chen, Y. W., Bi, X. W., Hu, R. Z., et al., 2012. Element Geochemistry, Mineralogy, Geochronology and Zircon Hf Isotope of the Luxi and Xiazhuang Granites in Guangdong Province, China: Implications for U Mineralization. *Lithos*, 150: 119–134. https://doi.org/10.1016/j.lithos.2012.06.025

Chung, S. L., Chu, M. F., Zhang, Y. Q., et al., 2005. Tibetan Tectonic Evolution Inferred from Spatial and Temporal Variations in Post-Collisional Magmatism. *Earth-Science Reviews*, 68(3/4): 173 – 196. https://doi.org/10.1016/j.earscirev.2004.05.001

Class, C., Goldstein, S. L., 1997. Plume-Lithosphere Interactions in the Ocean Basins: Constraints from the Source Mineralogy. *Earth and Planetary Science Letters*, 150(3/4): 245–260. https://doi.org/10.1016/s0012-821x(97)00089-7

Collins, W. J., Beams, S. D., White, A. J. R., et al., 1982. Nature and Origin of A-Type Granites with Particular Reference to Southeastern Australia. *Contributions to Mineralogy and Petrology*, 80(2): 189–200. https://doi.org/10.1007/bf00374895

Corfu, F., 2003. Atlas of Zircon Textures. *Reviews in Mineralogy and Geochemistry*, 53(1): 469–500. https://doi.org/10.2113/0530469

Cui, J. T., Wang, J. C., Bian, X. W., et al., 2007a. Zircon SHRIMP U-Pb Dating of the Dongbake Gneissic Tonalite in Northern Kangxiwar, West Kunlun. *Geological Bulletin of China*, 26(6): 726 – 729 (in Chinese with English Abstract)

Cui, J. T., Wang, J. C., Bian, X. W., et al., 2007b. Zircon SHRIMP U-Pb Dating of Early Paleozoic Granite in the Menggubao-Pushou Area on the Northern Side of Kangxiwar, West Kunlun. *Geological Bulletin of China*, 26(6): 710–719 (in Chinese with English Abstract)

DePaolo, D. J., Daley, E. E., 2000. Neodymium Isotopes in Basalts of the Southwest Basin and Range and Lithospheric Thinning during Continental Extension. *Chemical Geology*, 169(1/2): 157–185. https://doi.org/10.1016/s0009-2541(00)00261-8

Foley, S., Tiepolo, M., Vannucci, R., 2002. Growth of Early Continental Crust Controlled by Melting of Amphibolite in Subduction Zones. *Nature*, 417(6891): 837–840. https://doi.org/10.1038/nature00799

Griffin, W. L., Wang, X., Jackson, S. E., et al., 2002. Zircon Chemistry and Magma Mixing, SE China: *In-situ* Analysis of Hf Isotopes, Tonglu and Pingtan Igneous Complexes. *Lithos*, 61(3/4): 237–269. https://doi.org/10.1016/S0024-4937(02)00082-8

Hawkesworth, C. J., Turner, S. P., McDermott, F., et al., 1997. U-Th Isotopes in Arc Magmas: Implications for Element Transfer from the Subducted Crust. *Science*, 276(5312): 551 – 555. https://doi. org/10.1126/science.276.5312.551

Henan Institute of Geological Survey, 2005. Geological Survey Report for 1 : 250 000 of Yingjisha County (in Chinese)

Hoskin, P. W. O., Black, L. P., 2000. Metamorphic Zircon Formation by Solid - State Recrystallization of Protolith Igneous Zircon. *Journal of Metamorphic Geology*, 18(4): 423–439. https://doi.org/10.1046/j.1525-1314.2000.00266.x

Hoskin, P. W. O., Black, L. P., 2000. Metamorphic Zircon Formation by

Solid-State Recrystallization of Protolith Igneous Zircon. *Journal of Metamorphic Geology*, 18(4): 423–439. https://doi.org/10.1046/j.1525-1314.2000.00266.x

Hu, J., Wang, H., Huang, C. Y., et al., 2016. Geological Characteristics and Age of the Dahongliutan Fe-Ore Deposit in the Western Kunlun Orogenic Belt, Xinjiang, Northwestern China. *Journal of Asian Earth Sciences*, 116: 1–25. https://doi.org/10.1016/j.jseaes.2015.08.014

Hu, J., Wang, H., Mu, S. L., et al., 2017. Geochemistry and Hf Isotopic Compositions of Early Paleozoic Granites in Nanpingxueshan from the Tianshuihai Terrane, West Kunlun: Crust-Mantle Magmatism. *Acta Geologica Sinica*, 91(6): 1192–1207 (in Chinese with English Abstract)

Hu, X. Y., Guo, R. Q., Nuerkanati·Madayipu, et al., 2017b. Zircon U-Pb Dating, Petrology, Geochemistry of the Buya Pluton and Its MMEs in the Southern Margin of Tarim, Xinjiang. *Rock and Mineral Analysis*, 36(5): 538–550 (in Chinese with English Abstract)

Hu, X. Y., 2018. Petrogenesis and Tectonic Significance of Granitic Pluton and MMEs in the Eastern Segment of the Tiekelike, NW China: [Dissertation]. Xinjiang University, Urumchi (in Chinese with English Abstract)

Ji, W. H., Li, R. S., Chen, S. J., et al., 2011. The Discovery of Palaeoproterozoic Volcanic Rocks in the Bulunkuoler Group from the Tianshuihai Massif in Xinjiang of Northwest China and Its Geological Significance. *Science China Earth Sciences*, 54(1): 61–72. https://doi.org/10.1007/s11430-010-4043-7

Ji, W. H., Chen, S. J., Li, R. S., et al., 2018. The Origin of Carboniferous-Permian Magmatic Rocks in Oytag Area, West Kunlun: Back-Arc Basin? *Acta Petrologica Sinica*, 34(8): 2393–2409 (in Chinese with English Abstract)

Jia, R. Y., Jiang, Y. H., Liu, Z., et al., 2013. Petrogenesis and Tectonic Implications of Early Silurian High-K Calc-Alkaline Granites and Their Potassic Microgranular Enclaves, Western Kunlun Orogen, NW Tibetan Plateau. *International Geology Review*, 55(8): 958–975. https://doi.org/10.1080/00206814.2012.755766

Jiang, Y. H., Jiang, S. Y., Ling, H. F., et al., 2002. Petrology and Geochemistry of Shoshonitic Plutons from the Western Kunlun Orogenic Belt, Xinjiang, Northwestern China: Implications for Granitoid Geneses. *Lithos*, 63(3/4): 165–187. https://doi.org/10.1016/S0024-4937(02)00140-8

Jiang, Y. H., Liao, S. Y., Yang, W. Z., et al., 2008. An Island Arc Origin of Plagiogranites at Oytag, Western Kunlun Orogen, Northwest China: SHRIMP Zircon U-Pb Chronology, Elemental and Sr-Nd-Hf Isotopic Geochemistry and Paleozoic Tectonic Implications. *Lithos*, 106(3/4): 323–335. https://doi.org/10.1016/j.lithos.2008.08.004

Kemp, A. I. S., Hawkesworth, C. J., Foster, G. L., et al., 2007. Magmatic and Crustal Differentiation History of Granitic Rocks from Hf-O Isotopes in Zircon. *Science*, 315(5814): 980–983. https://doi.org/10.1126/science.1136154

King, P. L., White, A. J. R., Chappell, B. W., et al., 1997. Characterization and Origin of Aluminous A-Type Granites from the Lachlan Fold Belt, Southeastern Australia. *Journal of Petrology*, 38(3): 371–391. https://doi.org/10.1093/petroj/38.3.371

Li, T. F., Zhang, J. X., 2014. Zircon LA-ICP-MS U-Pb Ages of Websterite and Basalt in Kudi Ophiolite and the Implication, West Kunlun. *Acta Petrologica Sinica*, 30(8): 2393–2401 (in Chinese with English Abstract)

Li, X. H., Li, Z. X., Li, W. X., et al., 2007. U-Pb Zircon, Geochemical and Sr-Nd-Hf Isotopic Constraints on Age and Origin of Jurassic I- and A-Type Granites from Central Guangdong, SE China: A Major Igneous Event in Response to Foundering of a Subducted Flat-Slab? *Lithos*, 96(1/2): 186–204. https://doi.org/10.1016/j.lithos.2006.09.018

Li, Y. C., Xiao, W. J., Tian, Z. H., 2019. Early Palaeozoic Accretionary Tectonics of West Kunlun Orogen: Insights from Datong Granitoids, Mafic-Ultramafic Complexes, and Silurian – Devonian Sandstones, Xinjiang, NW China. *Geological Journal*, 54(3): 1505–1517. https://doi.org/10.1002/gj.3246

Liang, Q., Jing, H., Gregoire, D. C., 2000. Determination of Trace Elements in Granites by Inductively Coupled Plasma Mass Spectrometry. *Talanta*, 51(3): 507–513. https://doi.org/10.1016/s0039-9140(99)00318-5

Liao, S. Y., Jiang, Y. H., Jiang, S. Y., et al., 2010. Subducting Sediment-Derived Arc Granitoids: Evidence from the Datong Pluton and Its Quenched Enclaves in the Western Kunlun Orogen, Northwest China. *Mineralogy and Petrology*, 100(1/2): 55–74. https://doi.org/10.1007/s00710-010-0122-x

Linnen, R. L., Keppler, H., 1997. Columbite Solubility in Granitic Melts: Consequences for the Enrichment and Fractionation of Nb and Ta in the Earth's Crust. *Contributions to Mineralogy and Petrology*, 128(2/3): 213–227. https://doi.org/10.1007/s004100050304

Linnen, R. L., Keppler, H., 2002. Melt Composition Control of Zr/Hf Fractionation in Magmatic Processes. *Geochimica et Cosmochimica Acta*, 66(18): 3293–3301. https://doi.org/10.1016/s0016-7037(02)00924-9

Liu, X. Q., Zhang, C. L., Ye, X. T., et al., 2019. Cambrian Mafic and Granitic Intrusions in the Mazar-Tianshuihai Terrane, West Kunlun Orogenic Belt: Constraints on the Subduction Orientation of the Proto-Tethys Ocean. *Lithos*, 350/351: 105226. https://doi.org/10.1016/j.lithos.2019.105226

Liu, X., Zhu, Z. X., Guo, R. Q., et al., 2016. LA-ICP-MS Zircon U-Pb Dating and Its Geological Significance for Late Paleozoic Diabase from the West Part of Tiekelike Area, South Tarim. *Geological Sciences*, 3: 794–805 (in Chinese with English Abstract)

Liu, Y. S., Hu, Z. C., Gao, S., et al., 2008. *In situ* Analysis of Major and Trace Elements of Anhydrous Minerals by LA-ICP-MS without Applying an Internal Standard. *Chemical Geology*, 257(1/2): 34–43. https://doi.org/10.1016/j.chemgeo.2008.08.004

Liu, Y. S., Hu, Z. C., Zong, K. Q., et al., 2010. Reappraisement and Refinement of Zircon U-Pb Isotope and Trace Element Analyses by LA-ICP-MS. *Chinese Science Bulletin*, 55(15): 1535–1546. https://doi.org/10.1007/s11434-010-3052-4

Liu, Z., Jiang, Y. H., Jia, R. Y., et al., 2014. Origin of Middle Cambrian and Late Silurian Potassic Granitoids from the Western Kunlun Orogen, Northwest China: A Magmatic Response to the Proto-Tethys Evolution. *Mineralogy and Petrology*, 108(1): 91–110. https://doi.org/10.1007/s00 710-013-0288-0

Ludwig, K. R., 2003. User's Manual for Isoplot 3.00——A Geochronological Toolkit for Microsoft Excel. *Berkeley Geochronological Center Special Publication*, 4: 25–32

Luo, Y. Q., Qin, H. Y., Wu, T., et al., 2020. Petrogenesis of the Granites in the Yandangshan Area, Southeastern China: Constraints from SHRIMP U-Pb Zircon Age and Trace Elements, and Sr-Nd-Hf Isotopic Data. *Journal of Earth Science*, 31(4): 693–708. https://doi.org/10.1007/s12583-020-1295-9

Maniar, P. D., Piccoli, P. M., 1989. Tectonic Discrimination of Granitoids. *Geological Society of America Bulletin*, 101(5): 635–643. https://doi.org/10.1130/0016-7606(1989)1010635:tdog>2.3.co;2

Martin, H., Smithies, R. H., Rapp, R., et al., 2005. An Overview of Adakite, Tonalite-Trondhjemite-Granodiorite (TTG), and Sanukitoid:

Relationships and Some Implications for Crustal Evolution. *Lithos*, 79(1/2): 1–24. https://doi.org/10.1016/j.lithos.2004.04.048

McCulloch, M. T., Gamble, J. A., 1991. Geochemical and Geodynamical Constraints on Subduction Zone Magmatism. *Earth and Planetary Science Letters*, 102(3/4): 358–374. https://doi.org/10.1016/0012-821x(91)90029-h

Metcalfe, I., Henderson, C. M., Wakita, K., 2017. Lower Permian Conodonts from Palaeo-Tethys Ocean Plate Stratigraphy in the Chiang Mai-Chiang Rai Suture Zone, Northern Thailand. *Gondwana Research*, 44: 54–66. https://doi.org/10.1016/j.gr.2016.12.003

Middlemost, E. A. K., 1994. Naming Materials in the Magma/Igneous Rock System. *Earth-Science Reviews*, 37(3/4): 215–224. https://doi.org/10.1016/0012-8252(94)90029-9

Münker, C., Pfänder, J. A., Weyer, S., et al., 2003. Evolution of Planetary Cores and the Earth-Moon System from Nb/Ta Systematics. *Science*, 301(5629): 84–87. https://doi.org/10.1126/science.1084662

Pan, Y. S., 2000. Geological Evolution of the Karakorum and Kunlun Mountains. Science Press, Beijing (in Chinese with English Abstract)

Pearce, J. A., Harris, N. B. W., Tindle, A. G., 1984. Trace Element Discrimination Diagrams for the Tectonic Interpretation of Granitic Rocks. *Journal of Petrology*, 25(4): 956–983. https://doi.org/10.1093/petrology/25.4.956

Peccerillo, A., Taylor, S. R., 1976. Geochemistry of Eocene Calc-Alkaline Volcanic Rocks from the Kastamonu Area, Northern Turkey. *Contributions to Mineralogy and Petrology*, 58(1): 63–81. https://doi.org/10.1007/bf00384745

Plank, T., Langmuir, C. H., 1998. The Chemical Composition of Subducting Sediment and Its Consequences for the Crust and Mantle. *Chemical Geology*, 145(3/4): 325–394. https://doi. org/10.1016/s0009-2541(97)00150-2

Qin, J. H., Liu, C., Chen, Y. C., et al., 2019. Timing of Lithospheric Extension in Northeastern China: Evidence from the Late Mesozoic Nianzishan A-Type Granitoid Complex. *Journal of Earth Science*, 30(4): 689–706. https://doi.org/10.1007/s12583-018-0996-9

Robinson, A. C., Yin, A., Manning, C. E., et al., 2004. Tectonic Evolution of the Northeastern Pamir: Constraints from the Northern Portion of the Cenozoic Kongur Shan Extensional System, Western China. *Geological Society of America Bulletin*, 116(7): 953. https://doi.org/10.1130/b25375.1

Rubatto, D., Gebauer, D., 2000. Use of Cathodoluminescence for U-Pb Zircon Dating by Ion Microprobe: Some Examples from the Western Alps. Cathodoluminescence in Geosciences. Springer, Berlin Heidelberg. https://doi.org/10.1007/978-3-66 2-04086-7_15

Rudnick, R. L., Gao, S., 2003. Composition of the Continental Crust. Treatise on Geochemistry, Elsevier, Amsterdam. https://doi. org/10.1016/b0-08-043751-6/03016-4

Saunders, A. D., Storey, M., Kent, R. W., et al., 1992. Consequences of Plume-Lithosphere Interactions. *Geological Society*, *London*, *Special Publications*, 68(1): 41–60. https://doi. org/10.1144/gsl. sp. 1992.068.01.04

Sisson, T. W., Grove, T. L., Coleman, D. S., 1996. Hornblende Gabbro Sill Complex at Onion Valley, California, and a Mixing Origin for the Sierra Nevada Batholith. *Contributions to Mineralogy and Petrology*, 126(1/2): 81–108. https://doi.org/10.1007/s004100050237

Stepanov, A., Mavrogenes, J., Meffre, S., et al., 2014. The Key Role of Mica during Igneous Concentration of Tantalum. *Contributions to Mineralogy and Petrology*, 167(6): 1–8. https://doi. org/10.1007/s00410-014-1009-3

Sun, S. S., McDonough, W. F., 1989. Chemical and Isotopic Systematics of Oceanic Basalts: Implications for Mantle Composition and Processes. *Geological Society*, *London*, *Special Publications*, 42(1): 313–345. https://doi.org/10.1144/gsl.sp.1989.042.01.19

Tang, H. F., Zhao, Z. Q., Huang, R. S., et al., 1998. Primary Hf Isotopic Study on Zircons from the A-Type Granites in Eastern Jinggar of Xinjiang, Northwest China. *Acta Mineralogica Sinica*, 28: 335–342 (in Chinese with English Abstract)

Tang, Y. W., Cui, K., Zheng, Z., et al., 2020. LA-ICP-MS U-Pb Geochronology of Wolframite by Combining NIST Series and Common Lead-Bearing MTM as the Primary Reference Material: Implications for Metallogenesis of South China. *Gondwana Research*, 83: 217–231. https://doi.org/10.1016/j.gr.2020.02.006

Tatsumi, Y., Hamilton, D. L., Nesbitt, R. W., 1986. Chemical Characteristics of Fluid Phase Released from a Subducted Lithosphere and Origin of Arc Magmas: Evidence from High-Pressure Experiments and Natural Rocks. *Journal of Volcanology and Geothermal Research*, 29(1/2/3/4): 293–309. https://doi.org/10.1016/0377-0273(86)90049-1

Tiepolo, M., Bottazzi, P., Foley, S. F., et al., 2001. Fractionation of Nb and Ta from Zr and Hf at Mantle Depths: The Role of Titanian Pargasite and Kaersutite. *Journal of Petrology*, 42(1): 221–232. https://doi. org/10.1093/petrology/42.1.221

Wang, J., Hattori, K., Liu, J. G., et al., 2017. Shoshonitic- and Adakitic Magmatism of the Early Paleozoic Age in the Western Kunlun Orogenic Belt, NW China: Implications for the Early Evolution of the Northwestern Tibetan Plateau. *Lithos*, 286/287: 345–362. https://doi.org/10.1016/j.lithos.2017.06.013

Wang, J. C., Cui, J. T., Luo, Q. Z., et al., 2006. The Discovery and Tectonic Significance of a Small Branch Ocean Basin in Monggubao-Pushouyuan, Tethyan Ocean of Northern Kangxiwa, West Kunlun Mountain. *Geology of Shaanxi*, 24(2): 41–49 (in Chinese with English Abstract)

Wang, J. C., Han, F. L., Cui, J. T., et al., 2003. Geochemical Characteristics of Early Paleozoic Granites in the Pulu Area, Yutian, Xinjiang and Its Tectonic Significance. *Regional Geology of China*, 22(3): 170–181 (in Chinese with English Abstract)

Wang, J. P., 2008. Geological Features and Tectonic Significance of Melange Zone in the Taxkorgan Area, West Kunlun. *Geological Bulletin of China*, 27(12): 2057–2066 (in Chinese with English Abstract)

Wang, L. X., Ma, C. Q., Zhang, C., et al., 2014. Genesis of Leucogranite by Prolonged Fractional Crystallization: A Case Study of the Mufushan Complex, South China. *Lithos*, 206/207: 147–163. https://doi. org/10.1016/j.lithos.2014.07.026

Wang, Y. Y., Xiao, Y. L., 2018. Fluid-Controlled Element Transport and Mineralization in Subduction Zones. *Solid Earth Sciences*, 3(4): 87–104. https://doi.org/10.1016/j.sesci.2018.06.003

Wang, Z. H., 2004. Tectonic Evolution of the Western Kunlun Orogenic Belt, Western China. *Journal of Asian Earth Sciences*, 24(2): 153–161. https://doi.org/10.1016/j.jseaes.2003.10.007

Wang, Z. H., Sun, S., Li, J. L., et al., 2002. Petrogenesis of Tholeiite Associations in Kudi Ophiolite (Western Kunlun Mountains, Northwestern China): Implications for the Evolution of Back-Arc Basins. *Contributions to Mineralogy and Petrology*, 143(4): 471–483. https://doi.org/10.1007/s00410-002-0358-5

Watson, E. B., Harrison, T. M., 1983. Zircon Saturation Revisited: Temperature and Composition Effects in a Variety of Crustal Magma Types. *Earth and Planetary Science Letters*, 64(2): 295–304. https://

doi.org/10.1016/0012-821x(83)90211-x

Whalen, J. B., Currie, K. L., Chappell, B. W., 1987. A-Type Granites: Geochemical Characteristics, Discrimination and Petrogenesis. *Contributions to Mineralogy and Petrology*, 95(4): 407–419. https://doi.org/10.1007/bf00402202

Williams, I. S., Buick, I. S., Cartwright, I., 1996. An Extended Episode of Early Mesoproterozoic Metamorphic Fluid Flow in the Reynolds Range, Central Australia. *Journal of Metamorphic Geology*, 14(1): 29–47. https://doi.org/10.1111/j.1525-1314.1996.00029.x

Wu, F. Y., Jahn, B. M., Wilde, S. A., et al., 2003. Highly Fractionated I-Type Granites in NE China (I): Geochronology and Petrogenesis. *Lithos*, 66(3/4): 241–273. https://doi.org/10.1016/s0024-4937(02)00222-0

Wu, F. Y., Liu, X. C., Ji, W. Q., et al., 2017. Highly Fractionated Granites: Recognition and Research. *Science China* (*Earth Sciences*), 60(7): 1201–1219 (in Chinese with English Abstract)

Wu, F. Y., Liu, Z. C., Liu, X. C., et al., 2015. Himalayan Leucogranite: Petrogenesis and Implications to Orogenesis and Plateau Uplift. *Acta Petrologica Sinica*, 31(1): 1–36 (in Chinese with English Abstract)

Wu, F. Y., Wan, B., Zhao, L., et al., 2020. Tethyan Geodynamics. *Acta Petrologica Sinica*, 36(6): 1627–1674 (in Chinese with English Abstract)

Wu, Y. B., Zheng, Y. F., 2004. Genesis of Zircon and Its Constraints on Interpretation of U-Pb Age. *Chinese Science Bulletin*, 49(15): 1554–1569. https://doi.org/10.1007/bf03184122

Xiao, W. J., Hou, Q. L., Li, J. L., et al., 2000. Tectonic Facies and the Archipelago-Accretion Process of the West Kunlun, China. *Science in China Series D*: *Earth Sciences*, 43(1): 134–143. https://doi.org/10.1007/bf02911939

Xiao, W. J., Windley, B. F., Chen, H. L., et al., 2002. Carboniferous-Triassic Subduction and Accretion in the Western Kunlun, China: Implications for the Collisional and Accretionary Tectonics of the Northern Tibetan Plateau. *Geology*, 30(4): 295. https://doi.org/10.1130/0091-7613(2002)0300295:ctsaai>2.0.co;2

Xiao, W. J., Windley, B. F., Liu, D. Y., et al., 2005. Accretionary Tectonics of the Western Kunlun Orogen, China: A Paleozoic–Early Mesozoic, Long-Lived Active Continental Margin with Implications for the Growth of Southern Eurasia. *The Journal of Geology*, 113(6): 687–705. https://doi.org/10.1086/449326

Yang, J. H., Sun, J. F., Zhang, J. H., et al., 2012. Petrogenesis of Late Triassic Intrusive Rocks in the Northern Liaodong Peninsula Related to Decratonization of the North China Craton: Zircon U-Pb Age and Hf-O Isotope Evidence. *Lithos*, 153: 108–128. https://doi.org/10.1016/j.lithos.2012.06.023

Ye, H. M., Li, X. H., Li, Z. X., et al., 2008. Age and Origin of High Ba-Sr Appinite-Granites at the Northwestern Margin of the Tibet Plateau: Implications for Early Paleozoic Tectonic Evolution of the Western Kunlun Orogenic Belt. *Gondwana Research*, 13(1): 126–138. https://doi.org/10.1016/j.gr.2007.08.005

Yin, J., Xiao, W., Sun, M., et al., 2020. Petrogenesis of Early Cambrian Granitoids in the Western Kunlun Orogenic Belt, Northwest Tibet: Insight into Early Stage Subduction of the Proto-Tethys Ocean. *GSA Bulletin*, in press. https://doi.org/10.1130/b35408.1

Yin, R., Wang, R. C., Zhang, A. C., et al., 2013. Extreme Fractionation from Zircon to Hafnon in the Koktokay No. 1 Granitic Pegmatite, Altai, Northwestern China. *American Mineralogist*, 98(10): 1714–1724. https://doi.org/10.2138/am.2013.4494

Yuan, C., Sun, M., Zhou, M. F., et al., 2002. Tectonic Evolution of the West Kunlun: Geochronologic and Geochemical Constraints from Kudi Granitoids. *International Geology Review*, 44(7): 653–669. https://doi.org/10.2747/0020-6814.44.7.653

Yuan, C., Sun, M., Zhou, M. F., et al., 2003. Absence of Archean Basement in the South Kunlun Block: Nd-Sr-O Isotopic Evidence from Granitoids. *Island Arc*, 12(1): 13–21. https://doi.org/10.1046/j.1440-1738.2003.00376.x

Yuan, C., Sun, M., Zhou, M. F., et al., 2005. Geochemistry and Petrogenesis of the Yishak Volcanic Sequence, Kudi Ophiolite, West Kunlun (NW China): Implications for the Magmatic Evolution in a Subduction Zone Environment. *Contributions to Mineralogy and Petrology*, 150(2): 195–211. https://doi.org/10.1007/s00410-005-0012-0

Zhai, Y. Y., Gao, S., Zeng, Q. D., et al., 2020. Geochronology, Geochemistry and Hf Isotope of the Late Mesozoic Granitoids from the Lushi Polymetal Mineralization Area: Implication for the Destruction of Southern North China Craton. *Journal of Earth Science*, 31(2): 313–329. https://doi.org/10.1007/s12583-020-1277-y

Zhang, C. L., Li, Z. X., Li, X. H., et al., 2007a. An Early Paleoproterozoic High-K Intrusive Complex in Southwestern Tarim Block, NW China: Age, Geochemistry, and Tectonic Implications. *Gondwana Research*, 12(1/2): 101–112. https://doi.org/10.1016/j.gr.2006.10.006

Zhang, C. L., Ye, X. T., Zou, H. B., et al., 2016a. Neoproterozoic Sedimentary Basin Evolution in Southwestern Tarim, NW China: New Evidence from Field Observations, Detrital Zircon U-Pb Ages and Hf Isotope Compositions. *Precambrian Research*, 280: 31–45. https://doi.org/10.1016/j.precamres.2016.04.011

Zhang, C. L., Yu, H. F., Ye, H. M., et al., 2006. Aoyitake Plagiogranite in Western Tarim Block, NW China: Age, Geochemistry, Petrogenesis and Its Tectonic Implications. *Science in China Series D*: *Earth Sciences*, 49(11): 1121–1134. https://doi.org/10.1007/s11430-006-1121-y

Zhang, C. L., Zou, H. B., Ye, X. T., et al., 2018a. A Newly Identified Precambrian Terrane at the Pamir Plateau: The Archean Basement and Neoproterozoic Granitic Intrusions. *Precambrian Research*, 304: 73–87. https://doi.org/10.1016/j.precamres.2017.11.006

Zhang, C. L., Zou, H. B., Ye, X. T., et al., 2018b. Tectonic Evolution of the NE Section of the Pamir Plateau: New Evidence from Field Observations and Zircon U-Pb Geochronology. *Tectonophysics*, 723: 27–40. https://doi.org/10.1016/j.tecto.2017.11.036

Zhang, C. L., Zou, H. B., Ye, X. T., et al., 2018c. Timing of Subduction Initiation in the Proto-Tethys Ocean: Evidence from the Cambrian Gabbros from the NE Pamir Plateau. *Lithos*, 314/315: 40–51. https://doi.org/10.1016/j.lithos.2018.05.021

Zhang, C. L., Zou, H. B., Ye, X. T., et al., 2019b. Tectonic Evolution of the West Kunlun Orogenic Belt along the Northern Margin of the Tibetan Plateau: Implications for the Assembly of the Tarim Terrane to Gondwana. *Geoscience Frontiers*, 10(3): 973–988. https://doi.org/10.1016/j.gsf.2018.05.006

Zhang, C. L., Ma, H. D., Zhu, B. Y., et al., 2019a. Tectonic Evolution of the Western Kunlun—Karakorum Orogenic Belt and Its Coupling with the Mineralization Effect. *Geological Review*, 65(5): 1077–1102 (in Chinese with English Abstract)

Zhang, H. S., He, S. P., Ji, W. H., et al., 2016b. Implications of Late Cambrian Granite in Tianshuihai Massif for the Evolution of Proto-Tethy Ocean: Evidences from Zircon Geochronology and Geochemistry. *Acta Geologica Sinica*, 90(10): 2582–2602 (in Chinese with English Abstract)

Zhang, Q. C., Liu, Y., Huang, H., et al., 2016c. Petrogenesis and Tectonic Implications of the High-K Alamas Calc-Alkaline Granitoids at the

Northwestern Margin of the Tibetan Plateau: Geochemical and Sr-Nd-Hf-O Isotope Constraints. *Journal of Asian Earth Sciences*, 127: 137–151. https://doi.org/10.1016/j.jseaes.2016.05.026

Zhang, Q. C., Wu, Z. H., Chen, X. H., et al., 2019a. Proto-Tethys Oceanic Slab Break-Off: Insights from Early Paleozoic Magmatic Diversity in the West Kunlun Orogen, NW Tibetan Plateau. *Lithos*, 346/347: 105147. https://doi.org/10.1016/j.lithos.2019.07.014

Zhang, Q. C., Wu, Z. H., Li, S., et al., 2019b. Ordovician Granitoids and Silurian Mafic Dikes in the Western Kunlun Orogen, Northwest China: Implications for Evolution of the Proto-Tethys. *Acta Geologica Sinica-English Edition*, 93(1): 30 – 49. https://doi. org/10.1111/1755-6724.13760

Zhang, Z. W., Shen, N. P., Peng, J. T., et al., 2014. Syndeposition and Epigenetic Modification of the Strata-Bound Pb-Zn-Cu Deposits Associated with Carbonate Rocks in Western Kunlun, Xinjiang, China. *Ore Geology Reviews*, 62: 227 – 244. https://doi. org/10.1016/j. oregeorev.2014.04.001

Zhang, Z. W., Cui, J. T., Wang, J. C., et al., 2007b. Zircon SHRIMP U-Pb Dating of Early Paleozoic Amphibolite and Granodiorite in Korliang, Northwestern Kangxiwar, West Kunlun. *Geological Bulletin of China*, 26(6): 720–725 (in Chinese with English Abstract)

Zhang, Z. W., Wu, C. Q., Zhu, W. G., et al., 2019c. The Late Palaeozoic Back-arc Basin and metallogenesis in West Kunlun. The Ninth National Symposium on Mineralization Theory and Prospecting Methods, 444–445 (in Chinese)

Zhu, J. E., Li, Q. G., Chen, X., et al., 2018. Geochemistry and Petrogenesis of the Early Palaeozoic Appinite-Granite Complex in the Western Kunlun Orogenic Belt, NW China: Implications for Palaeozoic Tectonic Evolution. *Geological Magazine*, 155(8): 1641–1666. https://doi.org/10.1017/s0016756817000450

Zhu, J., Li, Q. G., Wang, Z. Q., et al., 2016. Magmatism and Tectonic Implications of Early Cambrian Granitoid Plutons in Tianshuihai Terrane of the Western Kunlun Orogenic Belt, Northwest China. *Northwestern Geology*, 49(4): 1–18 (in Chinese with English Abstract)